Author:
Kelly, David

Title:
Effects of Engine Location and Thrust on Aeroelastic Behaviour and Gust Response of a Flexible Bending-Torsional Wing

Effects of Engine Location and Thrust on Aeroelastic Behaviour and Gust Response of a Flexible Bending-Torsional Wing

David J Kelly

A dissertation submitted to the University of Bristol in accordance with the requirements for award of the degree of MSc Aerospace Engineering in the Faculty of Engineering

Text Word Count: 11,958

Abstract:

Lagrange and Rayleigh-Ritz analytical techniques were used to develop a four mode aeroelastic model of a simple rectangular flexible wing with a point mass and thrust system. This model was used to investigate the effects that aero-engines location have on flutter behaviour and gust response. It was found that increasing the size of the point mass had a stabilizing effect on flutter, whereas an increase in thrust had the opposite effect. Moving the mass along the span towards the leading-edge of the wing-tip provided greatest flutter stability but the variation in flutter speed was distinctly non-linear. Conversely, the leading-edge wing-tip was seen to be the most critical position of the thrust placement. With respect to gust response, an increase of both the external mass and thrust increased the deflection of the wing when placed towards the wing-tip. However, the smaller magnitude of external mass caused the greatest total wing deflection.

Author's declaration

I declare that the work in this dissertation was carried out in accordance with the requirements of the University's Regulations and Code of Practice for Research Degree Programmes and that it has not been submitted for any other academic award. Except where indicated by specific reference in the text, the work is the candidate's own work. Work done in collaboration with, or with the assistance of, others, is indicated as such. Any views expressed in the dissertation are those of the author.

SIGNED: ..... DATE: .....

Contents

Nomenclature	
a_w	Wing lift curve slope
$\boldsymbol{A}$	Inertial matrix
$\boldsymbol{A_{ex}}$	External store inertial matrix contribution
$\boldsymbol{B}$	Aerodynamic damping matrix
c	Wing chord length
$\boldsymbol{C}$	Aerodynamic stiffness matrix
e	Eccentricity ratio between flexural axis and aero centre
$\boldsymbol{E}$	Structural stiffness matrix
$\boldsymbol{E_{ex}}$	External store structural stiffness matrix contribution
EI	Flexural rigidity
$\boldsymbol{F_{gust}}$	Gust input column matrix
GJ	Torsional rigidity
I_w	Wing moment of inertia about the mass axis
I_{ex}	Moment of inertia of external point mass due to pendulum effect about the flexural axis
m	Mass per unit area
m_{ex}	External store mass
m_{LE}	Mass at chord leading edge
m_{TE}	Mass at chord trailing edge
$M_{\dot{\theta}}$	Oscillatory aerodynamic moment derivative about the lateral axis with respect to pitch rate
P	External store follower-force
q_j	Generalized coordinates
Q_{qi}	Generalised forces
Q	System matrix of aeroelastic equation
R	Pylon length
r	Chord-wise distance of flexural axis to external store
s	Wing semi-span
T	System kinetic energy
U_{ds}	Design gust velocity
U_{ref}	Gust reference velocity
W_a	Work done by aerodynamic forces and moments
W_P	Work done by follower force thrust
x_f	Chord-wise position of flexural axis
x_m	Chord-wise position of mass axis
x_{ex}	x distance to external store
y_{ex}	y distance to external store
z	Wing z direction deformation
z_{ex}	External store z movement
λ_j	System matrix eigenvalues
θ	Wing twist deformation
$\omega_g(t)$	Instantaneous gust magnitude

1. Introduction

1.1. Overview of Aeroelasticity

Aeroelasticity can be defined as the scientific field which studies the interaction between aerodynamic, elastic, and inertial forces. It is generally divided into the two classes of static and dynamic aeroelasticity. This interaction of forces and disciplines is most commonly depicted as the Collar aeroelastic triangle shown in figure 1[1]. It shows that for static aeroelastic problems, only aerodynamic and elastic forces must be present, whereas for dynamic aeroelastic problems all three forces are required. The disciplines of mechanical vibration, and stability and control, also concern two of these three forces.

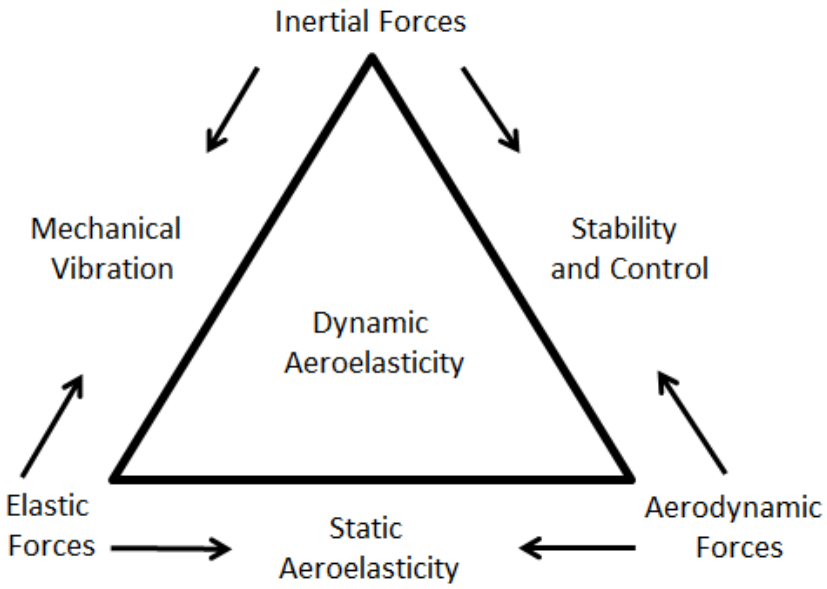

Figure 1-Collar's Aeroelastic Triangle

The three forces of the aeroelastic triangle each result in a corresponding load which acts on the aircraft, and so the closely related loads triangle is derived. The loads triangle is shown in figure 2 (Wright & Cooper, 2007). In the centre of the loads triangle, gust and turbulence loads correspond to dynamic aeroelasticity and involves and interaction from all three forces. Taxiing aircraft experiencing ground manoeuvre loads are subjected to elastic and inertial forces. These types of loads correspond to the domain of mechanical vibration. Equilibrium or steady manoeuvre loads are generated by a combination of elastic and aerodynamic forces and refers to longitudinal and lateral manoeuvres such as a steady pull up where the pitch rate of change is zero. These loads correspond to the domain of static aeroelasticity. Finally, dynamic manoeuvres such as pitch, yaw, and roll accelerations are non-

zero, imparting inertial and aerodynamic forces. The discipline of stability and control deals with loads of this nature.

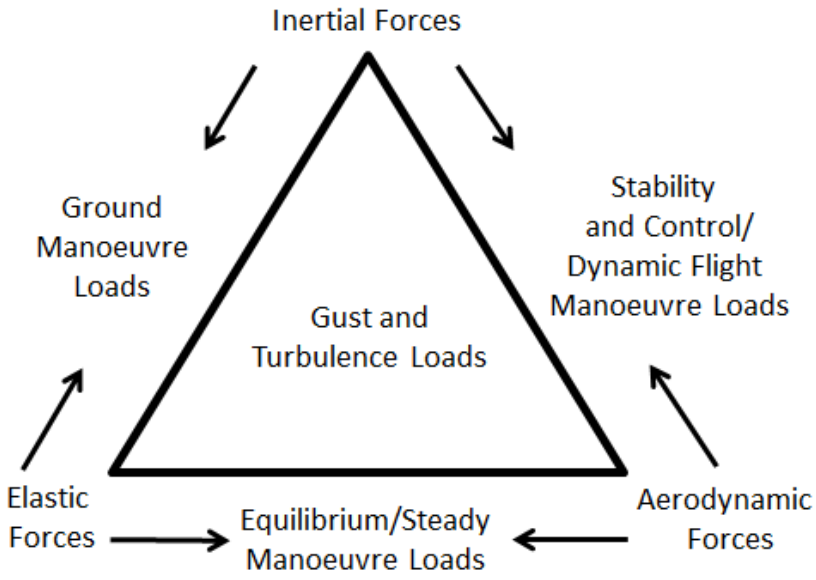

Figure 2-Loads Triangle

Although aeroelastic phenomenon has plagued aviation since the beginning of powered heavier-than-air aircraft, aeroelasticity only developed to the significant field it is today during the 1920's and 30's with the development of mature cantilever monoplane aircraft of that era. Development accelerated further with the advent of the Second World War and the associated push for increased speed and loads. Although the monoplane design was in use at the beginning of the First World War, it virtually disappeared by the war's end. It is now known that the lack of torsional stiffness criteria which caused the disuse of this design for military aircraft, favouring the biplane for its structural strength which allowed superior manoeuvrability but at the expense of reduced speed.

The design of aircraft is shaped by aeroelastic phenomenon in many significant ways. Divergence is a static instability whereby an incremental change in wing twist deflection results in an increase of aerodynamic forces therefore increasing wing twist further until structural failure occurs. This phenomenon affects criteria for the required torsional stiffness of wings and the distance between the centre of twist and aerodynamic centre. Control effectiveness and reversal became prominent problems during the early jet age and the popular rise of wing sweep required by the increased speed. This twisting alters the lift distribution in such a way as to reduce or even reverse the desired control output. The static shape of the wing is crucial to its aerodynamic performance, which is compromised

with such wing twist. The phenomenon again dictates the amount of torsional stiffness required for the lifting surfaces.

Dynamic aeroelastic phenomenon includes flutter and gust loads. Flutter occurs as a result of elastic deflections of wings or other surfaces and structures interacting with the aerodynamic forces in an oscillatory manor. This unfortunate interaction causes aerodynamic loads to amplify structural deflection with each oscillation and can potentially lead to structural failure. Flutter has one of the most far reaching influences on aircraft design from wing planform shape, inertial mass distribution, and stiffness strengths.

Within industry, there are multiple ways in which gusts and gust loads are simulated and designed for. Historically, modelling gusts as a single or discrete gust of a given profile has been used for many years and is part of the airworthiness regulations [2, 3]. The sharp-edged gust whereby the aircraft, initially in still air, abruptly enters a uniform velocity field, proved appealing due to its simplicity. With realisation that real gust velocities build up to a maximum value over a period of time, the sharp-edged gust fell out of favour and airworthiness requirements adapted on the assumption that gust velocity increased to a maximum in a linear fashion, known as the graded or ramp gust. However, more recently the discrete gusts are more commonly represented by the '1-cosine' gust. The approach taken in this thesis is to use a family of these 1-cosine gusts varying in maximum intensity and duration. This approach correlates more closely to modern industrial practice.

Air transport plays a huge sociological and economical role in the developed and developing world. With the huge demand in Europe for passenger mobility and air freighted goods, the Flighpath2050 initiative defines a number of aims for European aviation to be met by 2050[4]. These targets set out ambitious targets focused around societal needs, industrial leadership, environmental goals, safety standards, and research. A European air traffic control system is to be developed capable of handling 25 million flights per year. It is aimed for 90% of European travellers to be capable of completing their full journey within a 4 hour time frame and all flights arriving within 1 minute of the planned arrival time. Industrial aims include a highly competitive aviation industry carving out 40% of the global aviation market and increasing the efficiency in design, manufacturing, and development with a 50% reduction in certification costs. The cost of fossil fuels to the earth is now well understood and with Europe continuing to lead the way in terms of sustainability and environmentally friendly systems, reducing the impact air traffic in Europe has to the environment is of increasing importance. Flightpath2050 aims to reduce each passenger's carbon dioxide impact by 75% and nitrogen oxide emissions by 90%. Aircraft are to become emission free during taxing manoeuvres and aero structures and components are manufactured to be completely recyclable at the end of the product life cycle.

Europe is also aiming to become world leading in alternative fuels and atmospheric research. In terms of safety, air transport within Europe aims to see less than one accident per ten million commercial aircraft flights and fully secured global high bandwidth air transport system and data network hardened and resilient by design to cyber-attacks. A multi-disciplinary network is to be formed promoting collaboration between industry, universities, and research institutes. Public and private stakeholders are to jointly define research and innovation strategies. Aerospace related university courses are to be highly relevant to the industry needs with students attracted to careers in aviation. A comparable initiative is also taking place in the UK [5].

In the U.S. similar initiatives have been defined [6, 7]. The N+3 Aircraft Concept Designs and Trade Studies report outlines research carried out as joint projects between industry and NASA. The collaboration aims to pursue revolutionary conceptual designs of subsonic commercial transport aircraft entering service for 2035. Multifaceted improvements were identified in terms of aerodynamics, propulsion, operations, and structures. From this assessment, two conceptual designs were identified. The first of these is the so called Double bubble fuselage concepts, the second being the Hybrid Wing Body concept. These designs both help meet the goals set out by the N+3 report which focuses on reducing fuel burn, noise, and chemical emissions harmful to the environment. The Double Bubble design is predicted to reduce fuel burn by over 70%. From the N+3 study, a recommendation was outlined to carry out a follow-on study looking into alternative fuels and energy sources. This N+4 report focused on technologies appropriate to aircraft operational in the 2040 time frame. These technologies include hydrogen, battery electric hybrids, boundary layer ingestion propulsion, and un-ducted fans.

It is known from the classic Breguet range equation that for a given speed, range can only be increased in three ways. Firstly, is to improve the aerodynamics in the form of increasing lift and reducing drag simultaneously. Secondly, is to reduce the structural weight of the aircraft. Finally, range can be increased by improving engine efficiency. With the aerospace industry pushing for ever greater efficiency in the form of structural weight reduction, recent techniques such as FEA and additive manufacturing, wing structures are becoming lighter and made from less material. As a result, they are becoming less rigid, bringing a renewed emphasis to aeroelasticity, particularly the risk of aeroelastic flutter. Although there have been numerous studies and literature on the now old problem of flutter of slender beams and wings, there is relatively little published study on the role wing-mounted engines play in this aeroelastic phenomenon. Since external stores are common to many types of aircraft, civil and military, this topic has become of special interest in aeroelasticity. The past 15 years has seen work carried out looking into using aeroelastic deflection to an advantage for improving performance

and minimising environmental impact [8, 9, 10, 11]. It is for these reasons that the modelling of aero engines and their effects on the aeroelastic behaviour of aircraft wings is of huge importance.

Aeroelastic flutter is an instability which can potentially lead to structural failure of lifting surfaces. The conventional solution to this problem is to increase the stiffness of these lifting surfaces so as to sufficiently delay airspeed or dynamic pressure boundaries of flutter to outside of that of the normal flight envelope. However, this safety margin, in the form of structural stiffness, adds precious weight to the aircraft at the cost of fuel and efficiency. The aerospace industry is pushing for ever greater efficiency in attempts to relieve the impact on the environment. Recent attempts at improving designs have seen slender, more flexible wings with lower drag and of lighter weight. This has brought aeroelastic phenomenon such as flutter into increasing concern. Of equal concern is the deformation of such flexible wings due to gust inputs.

Higher flutter speeds and lower gust loads enable lighter aircraft designs as less structure is required to achieve the same flutter and loads constraints, thus significantly improving the fuel efficiency of aircraft. There is much recent interest in hybrid electric / all-electric aircraft including distributed propulsion concepts such as NASA's X-57 seen in figure 3[12]. The effect of the positioning of the propulsion sources on the loads and aeroelastic behaviour is an area that needs to be considered, and this thesis is the first step towards this goal by only considering the position and size of a single engine on a flexible wing.

Figure 3-NASA's X-57 Electric Research Aircraft

1.2. Thesis Aims

The aims of this thesis can be broadly outlined as follows;

- Investigate the effects of the engine mass and thrust wing position and magnitude have on aeroelastic flutter and divergence speed.
- Investigate the effects of the engine mass and thrust wing position and magnitude have on the deflection of the wing during a gust response.
- Bring together a summary of past work surrounding the topic of external-store effects on flutter stability and highlight any themes and patterns that become apparent. Compare with the findings of the computations in this thesis.

1.3. Structure of Thesis

This thesis will present the results of research carried out into the flutter and gust stability of a wing with different external store configurations and positions. Section 2 of this thesis gives a broad overview of the previous work on this topic, outlining the method used and relevant conclusions. The governing equations of the model used for this investigation is detailed in section 3. The results pertaining to the effects the external store has on flutter speed and gust response are presented on section 4 and 5 respectively. Finally, a discussion of these results and the main conclusions will be summarised in section 6.

2. Literature Review

This section presents a survey of previous work relevant to the topic of this thesis and is roughly categorised starting with the earliest paper on this topic along with papers on straight wings with the external store position limited to the wing-tip. Next, previous work is presented on straight, unswept, untapered wings but with a focus on the effects of span and chord wise position of the external store. These sections are followed by work which looks at the effects of external stores on swept wings. The section then goes on to present work which focused on composite wings followed by a small number of recent papers using non-linear techniques. Previous work looking at flutter of wings with external stores is summarised in table 1. Finally, work focused around the topic of gust response of wing/store systems is presented.

One of the first papers to consider specifically the effects external stores have on flutter was by Goland & Luke [13] using differential equations of motion of the wing via the extended Galerkin's Method. These results are consistent with solutions of other papers using alternative numerical and analytical methods. The first experimental work on the subject was done by Runyan & Sewal [14] who later went on to complement these experimental results with a differential equation analysis and a comparison between the two[15, 16]. These experimental results also showed external mass to be immaterial on divergence speed.

A few papers focus on the effects of placing the mass and follower force at the wingtip [17] using aerodynamic strip-theory and Frobenius method, found that for a cantilever wing in airflow, subjected to a thrust follower force and point mass on the wing-tip, the thrust plays a destabilising role, whereas the mass plays a stabilising role in all cases. These findings are in agreement with the results of this present thesis.

For high aspect-ratio wing with a tip follower-force and using finite-state unsteady aerodynamics, Hodges[18] looked at how the flutter boundary varied with the ratio of bending to torsional stiffness, finding that the thrust follows a complicated relationship with this ratio. More generally, a decrease in flutter speed was seen as tip follower force was increased. He found that for bending to torsional stiffness ratios below or equal to five, to a certain point, increasing follower force will actually increase flutter speed.

Hodges' results contrasted to those of Feldt [17] in that Feldt used a bending to torsional stiffness ratio for which the follower force happened to destabilise flutter.

Much of the previous work, however, looks at simulating straight wings with external stores and varies store location as well as the magnitude of the store mass and follower force.

Runyan [19] continued Hodges' work, looking this time at external store span-wise and chord-wise location, as well as a store attachment method to achieve passive control and so increase flutter speed. Results were presented for the two cases of mass attached via rigid and flexible store pylon. Two-dimensional incompressible, unsteady aerodynamic theory was used for the aerodynamic model and Lagrange's method formed the basis of the governing equations. For a rigidly attached mass, flutter speed drops as the mass is moved to the mid-span and then increases back to clean wing flutter speed. For a flexible pylon, moving the mass toward the wing-tip continuously increased the flutter speed relative to the clean wing flutter speed.

Using Hamilton's principle and unsteady aerodynamic pressure loading, Fazelzadeh et al [20] considered a straight wing with an external store consisting of a follower force as well as a point mass. The flutter boundary was validated with results from Hodges and a very good agreement was seen. With a mass placed at the leading edge 80% span, increasing the mass reduced the flutter boundary of the wing/mass system. As the span-wise position of the mass is moved, as seen with Runyan in 1980, the flutter speed drops until the mid-span position is reached and then recovers towards the wing-tip. Moving the mass towards the wing-tip was seen to continuously decrease the flutter frequency. Regarding the chord-wise mass location, moving the mass forward towards the leading-edge increases flutter speed. Span-wise movement of the follower force decreases the flutter speed when moved to the wing-tip, but had no effect on flutter frequency which stayed virtually constant. The flutter frequency remained constant with changes in chord-wise position of the mass and follower force. The effect of changing the bending to torsional stiffness ratio was also investigated, finding that the flutter boundary was reduced as this ratio was increased.

Using a finite element wing/store model and unsteady aerodynamics via the doublet lattice method Wang [21] looked at the role of external store location but restricted the store movement to 30% to 35% span-wise and -4% to 8% chord-wise movement relative to the leading edge. The external store consisted of both point mass and follower forces. The span-wise external store movement showed a marginal reduction in flutter speed and engine pitch damping. The chord-wise movement had little effect on the flutter speed but increased the engine pitch damping. It was noted that as the chord-wise location of the external store was moved, the length of the flexible pylon changed which was shown to have an effect on the results.

An aeroelastic response of a wing/store system subjected to constant and different types of time-dependent thrusts was carried out by Mazidi et al [22]. Governing equations were derived through Lagrange with an unsteady aerodynamics model in terms of the Wagner's function. In addition to the chord and span-wise location, the effects of vertical location of the external store were also investigated. Considering just the follower force location, movement from root to wing-tip or trailing edge to leading edge was seen to destabilise the flutter response of the wing. For a point mass, 70% wing span location was seen to be the most critical position in terms of flutter stability. Further, moving the point mass chord-wise position towards the leading edge had a stabilising effect. Generally, the vertical location of the external store had negligible effects.

More recently, the research focus has shifted more towards modelling of swept wings looking at the effects of common flight manoeuvres in an attempt to improve the relevance of the results. A majority of this work was carried out by Mazadi and Fazelzadeh who favoured the use of Hamilton's principle for the governing structural equations coupled with Peter's finite state aerodynamics.

Mazadi & Fazelzadeh [23] considered the case of a swept wing carrying twin external powered stores. This work showed that for a configuration of 30 degrees sweep and mass stores at 30% and 70% span respectively, the flutter boundary decreased as the engine thrust was increased. The thrust was also seen to reduce the flutter speed for the case of a straight wing, being particularly sensitive to the thrust of the outboard engine. The outboard store was seen to have a greater effect on the flutter frequency compared to the inboard engine and the flutter frequency also varied with wing sweep. For a straight wing, increasing the outer engine thrust increased flutter frequency. Conversely, for 45 degree wing sweep, increasing the outer engine thrust would reduce the flutter frequency. Increasing the mass of the external stores also reduced flutter speed and frequency. The paper also looked at the effects of varying the location of the outboard engine from mid-span to wing-tip. The flutter speed decreases slowly until the engine reached around the 75% span and from there the flutter speed recovers. Increasing the mass of the external stores also reduced the flutter speed and corresponding frequency.

Fazelzadeh et al [24] explored the effects of a simple roll manoeuver on flutter velocity of a shear deformable swept clean wing. For the classical, non-shear deformable wing, sweep was seen to increase the flutter speed with forward sweep giving the greatest increases. An increase in the rolling angular velocity decreased both the flutter speed and velocity. With shear deformability introduced, the same pattern of results were seen but with slightly reduced flutter speed and frequency. Increasing aspect ratio was also seen to reduce flutter speed and frequency.

This investigation was extended by Mazadi et al [25] to include a wing with an external store. The flutter boundary was validated against Hodges results, and the effects of rolling angular velocity investigated for a wing swept at 30 degrees with a mass located at the mid-span quarter chord. The flutter speed decreased as the engine was moved along the span, in contrast to this work, but increasing the wing-tip thrust marginally decreased the flutter speed. Overall, the results showed that the extent to which roll angular velocity effects flutter was itself dependent on the magnitude of the external store mass and where it is located on the wing. Furthermore, this paper also looked at the influence of the distance between the aircrafts centre of gravity and the wing root, with results showing that distance significantly contributed to the flutter speed and frequency values.

Fazelzadeh et al [26] performed an aero elastic analysis of unrestrained wing/fuselage system with external stores performing a simple roll manoeuvre. Investigations into the effects of the external stores focused on span-wise position, but only two different chord-wise cases were investigated. The first case placed the store centre of gravity at the flexural axis, and the second case placed it at 63% behind the flexural axis. Again, the critical position of the external mass was around the mid-span. Increasing the distance of the mass from the flexural axis decreased the flutter speed but when placed on the flexural axis, the flutter speed increased significantly towards the wing-tip. The flutter frequency steadily decreased as the mass is moved span-wise. Increasing the mass was seen to confine the flutter stability region and reduce the frequency in the usual manor. Moreover, the effect of fuselage mass was explored and it was found that increasing the fuselage the mass increased the flutter speed with the chord-wise position relative to the flexural axis playing a significant role. With the mass placed at the mid-span, the roll angular velocity had very little effect with the exception of very high values which reduced the flutter speed. The paper also looked at the case of an unrestrained aircraft with stores on both wings and the effects of moving the stores away from the wing root. In this case it was seen that moving the stores towards the wing-tip increased flutter speed and reduced flutter frequency for all values of roll velocity, with higher values of roll velocity reducing this increase. These results outline the important role wing sweep plays in relation to the flutter behaviour along with the external store location.

Some papers have looked at composite wings with anisotropic material properties. Gern [27] looked at the effect of wing sweep and multiple external mass stores arrangements on a shear deformable composite wing. Governing equations were set up using Hamilton's variational Principle and aerodynamics provided by aerodynamic strip theory solved via the extended Galerkin method. Gern's results show that introducing shear deformability to the model slightly reduces flutter speed. With the use of 3D plots of flutter speed to mass location, the leading edge wing-tip increased the flutter speed

the most significantly. In terms of flutter frequency, the chord-wise position was seen to have little effect, whereas moving the mass away from the wing root steadily reduced flutter frequency. Wing sweep would have the usual effect of increasing flutter speed for all types of store arrangements, particularly for the forward sweep case. This paper also concluded that the store had no effect on divergence speed which is a function of wing stiffness.

A free vibration dynamic response of a thin-walled anisotropic composite wing with an external mass store was investigated by Librescu & Song [28]; transverse shear and warping were also integrated into the model. Again, the governing equations were derived using Hamilton's principle and solved with extended Galerkin method. The wing/mass system was subjected to a set of time-dependent loads from which the dynamic response was presented. One of the more relevant results was that increasing the wing-tip mass increased the twisting deflection in response to a sonic-boom type input under supersonic configuration. This paper also looked into the effects of composite layer ply angle on the stiffness of the wing.

Furthermore, Mazidi & Fazelzadeh [29] carried out a flutter analysis of the effects of a powered external store on a composite swept wing. Governing equations and unsteady aerodynamics model was obtained using Hamilton's principle and modified Peter's pressure loading for swept wings. As with the results for isotropic metal wings, increasing the sweep improved the flutter stability significantly. Similar to other work by these authors, the results pertaining to the effects of mass generally show that the external store mass play a destabilising role, with the span-wise movement having very little effect, contradicting the results of this present work. More agreement is found with the results from the effects of the external store thrust. Moving the thrust towards the leading or trailing edge reduces the flutter stability, particularly when moved span-wise towards the wing-tip. Both upward and downwards horizontal movement of the external store, for mass and/or thrust, reduced the flutter speed.

Similarly, Amoozgar et al [30] looked at the flutter characteristics of a composite wing system with a movable external mass using Lagrange and Ritz methods to derive the governing equations. Wagner's function was used for the incompressible unsteady aerodynamics. As well as the effects of external mass magnitude and location, the effects of the composite layer angles were also considered. For a wing-tip mass located on the elastic axis, increasing the mass generally decreases the flutter speed regardless of the composite layer angle, but particularly those angled at 0 and 45 degrees. The composite layer ply angle was seen to have a significant effect on the flutter speed. Regarding the chord-wise position, the elastic axis was shown to be the most unstable location for mass placement along the wing-tip. How the flutter speed varies with span location was seen to depend heavily on how

the composite layers are were angled, but generally, the 70% span location was the most stable position. The wing-tip position was the worst case for all composite layer angles.

Many recent aeroelastic works have focused on applying non-linear techniques to model wings with external stores and investigate the aeroelastic characteristics [31, 32]. One of the first to apply these techniques to a cantilever wing with an external store was Kim & Strganac [33]. Also, Zafari [34] using a non-linear structural model along with incompressible unsteady aerodynamics, found that increasing the follower force decreased the flutter speed and that the wing-tip was the critical location.

Table 1 presents an overview perspective of the previous work referenced above relating to flutter speed variation with external store characteristics and position. A wide selection of modelling approaches has been used on wings of various aspect ratios. Results for the effects and mass and thrust are separated into two separate columns and colour coded based on how much agreement was found with this present work, with red indicating disagreement and green indicating agreement. It should be noted that this table and comments relate to general patterns seen from varying the characteristic and location of the external store. General patterns can be said to agree even if specific flutter speeds calculated for similar wing parameters may vary.

It can be seen that for the work which considered a follower force or external store thrust in the model, excellent agreement is found in that thrust destabilises flutter, particularly as moved span-wise towards the wing-tip and forward towards the leading edge. In terms of mass size and location, the results can be seen to fall into two relatively distinct categories, with the exception of a few results falling outside of these general patterns. The first category of results shows that increasing the wing mounted mass to improve flutter stability and that moving this mass towards the leading edge wing-tip causes a continuous increase in flutter speed. This general pattern agrees with the results of this present work. The second category is characterised as mass size playing a destabilising role in relation to flutter. Particularly characteristic is how flutter speed varies with mass span-wise movement. As the mass is moved from the wing root, flutter speed is seen to steadily decrease, with the critical span station located around the 60% wing span position. From there, flutter speed then steadily increases recovering to clean wing flutter speed as the mass reaches the wing-tip. This second general pattern contrasts with the results of this present thesis.

Reference	Sweep	AR	Material	Aerodynamics	Governing Equations	Results Agreement-Mass	Results Agreement-Thrust	Comments
(Feldt, 1974)	Straight	4	Isotropic	Aerodynamic strip theory	Frobenius method			Tip mass increases flutter speed, and tip thrust reduces flutter speed.
(Runyan, 1980)	Straight	N/a	Isotropic	Two-dimensional incompressible, Unsteady aerodynamic theory	Lagrange		N/a	For rigid mass pylon, flutter speed drops when placed around the mid-span, then recovers to clean wing flutter speed at the wing tip. However, for flexible pylon flutter speed consciously increases as mass is moved towards wing tip.
(Gern, 1998)	Variable	6.16	Composite	Aerodynamic strip theory	Hamilton's Principle		N/a	Moving mass towards LE wing tip improves flutter speed.
(Hodges, 2001)	Straight	16	Isotropic	finite-state aerodynamic modelling	nonlinear mixed finite element method	N/a		Wing tip trust reduces flutter speed.
(Librescu & Song, 2008)	Straight	variable	Composite	Time dependent Heaviside functions	Hamilton's principle		N/a	Increasing store mass reduces deflection aplitude, but increases wing twisting amplitude response to sonic boom type input force.
(Fazelzadeh, et al, 2009)	Straight	6	Isotropic	Unsteady aerodynamic loading	Hamilton's principle			Flutter speed drops as mass is placed around the mid span, then increases to clean wing flutter speed as wing tip is approached. Flutter speed is increased as mass is moved toward leading edge. Thrust reduces flutter speed with critical location at wing tip.
(Mazidi & Fazelzadeh, 2010)	Variable	N/a	Composite	Peter's unsteady aerodynamic pressure loadings	Hamilton's principle			Flutter speed drops as mass is placed around the mid span, then increases to clean wing flutter speed as wing tip is approached. Flutter speed is increased as mass is moved toward leading edge. Thrust reduces flutter speed with critical location at wing tip
(Amoozgar, 2011)	Straight	16	Composite	Wagner's function	Lagrange		N/a	Wing tip mass reduces flutter speed. Flutter speed increases as mass is moved towards leading or trailing edge and when mass is placed around 60-80% span location along the elastic axis.
(Mazadi, et al, 2011)	30deg	N/a	Isotropic	Peter's unsteady aerodynamic pressure loadings	Hamilton's principle			Flutter speed drops as mass is placed around the mid span, then increases to clean wing flutter speed as wing tip is approached. Flutter speed is increased as mass is moved toward leading edge. Thrust reduces flutter speed with critical location at wing tip
(Mazidi, et al., 2013)	Straight	N/a	Isotropic	Wagner's function	Lagrange			Flutter speed drops as mass is placed around the mid span, then increases to clean wing flutter speed as wing tip is approached. Flutter speed is increased as mass is moved toward leading edge. Thrust reduces flutter speed with critical location at wing tip
(Mazadi & Fazelzadeh, 2013)	30deg	6.67	Isotropic	Peter's finite-state aerodynamic model	Hamilton's principle			Increasing mass of external stores placed at 30% & 70% span reduces flutter speed. Thrust reduces flutter speed.
(Fazelzadeh, et al, 2015)	N/a	N/a	Isotropic	Theodorsen unsteady aerodynamics	Galerkin's method		N/a	For mass placed along the flexural axis wing tip, flutter speed is increased significantly. Drop in flutter speed as mass is moved along the mid span and away from flexural axis.
(Zafari, 2017)	Straight	16	Isotropic	incompressible unsteady aerodynamic model	Hamilton's principle	N/a		Thrust decreases flutter speed and most critical placement is wing tip position.

Table 1 – References with Flutter Speed Results Summary

Only a limited amount of work has focused on gust response of wing/store systems. Becker [35] modelled a delta winged fighter aircraft with a missile type external store positioned at the wing-tip in a low altitude, high speed configuration. Results were obtained with solution of both the linear and non-linear flight dynamic equations of motion in the time and frequency domain respectfully. The paper focused on predicting gust loads and the effects of applying a gust load alleviation system as well as ride comfort. Very high acceleration of the wing-tip missile was caused by discrete gusts, particularly for the short gust length case. The system was seen to benefit from the gust load alleviation system.

Suppression of gust effects on a wing/store system with the use of a controller was studied more recently in 2017 by Fazelzadeh et all [36]. The system considered is a two dimensional aerofoil with external mass store. The governing equations obtained through Lagrange equation of motion and are nonlinear. The paper looked into the effects of airflow velocity, random gust input, controller gain, and stiffness of the system on the pitch angle and plunge displacements of the aerofoil and external store. The active controller was seen to significantly improve the system in terms of reducing displacements.

3. Model and Governing Equations

An assumed modes wing/store structural model and unsteady aerodynamic model is developed in order to investigate the aeroelastic characteristics of the system. The origin of the co-ordinate system employed is placed at the leading edge of the wing root.

3.1. Wing-Eternal Store Model

The Rayleigh-Ritz method is used to represent the deformation of the two-dimensional wing system. At any given point on the wing, the deformation $z(x, y, t)$ through bending and twisting is given by the following series

$$z(x, y, t) = \sum_{j=1}^{N} \psi_j(x, y)\, q_j(t) \tag{1}$$

In this series $\psi_j(x, y)$ is one of N assumed deformation shapes, and $q_j(t)$ are the generalised coordinate coefficients of unknown magnitude. Shape functions are assumed which satisfy the following boundary conditions

$$z = \dot{z} = 0 \; at \;\; y = 0 \tag{2}$$

that is, there is no deflection or slope at the wing root. In this analysis, four mode shapes, two bending and two torsion, are assumed such that

$$z(x, y, t) = y^2 q_1 + y^3 q_2 + y\big(x - x_f\big) q_3 + y^2\big(x - x_f\big) q_4 \tag{3}$$

$$\theta = y q_3 + y^2 q_4 \tag{4}$$

The external store is positioned at $(x_{ex},\ y_{ex})$ and the deflection at this point can be denoted as

$$z_{ex} = z(x_{ex},\ y_{ex}, t) \tag{5}$$

In terms of these generalised coordinates q_j and neglecting the damping term, Lagrange's equation takes the form

$$\frac{d}{dt}\left(\frac{\partial T}{\partial \dot{q}_j}\right) - \frac{\partial T}{\partial q_j} + \frac{\partial U}{\partial q_j} = Q_j = \frac{\partial}{\partial}\frac{(\delta W)}{\big(\delta q_j\big)} \quad for\ j = 1, 2, \dots, N, \tag{6}$$

The expression for the kinetic energy of the system has four contributing components; the motion associated with the deflection of the wing, movement of the external mass in the z-direction, the moment of inertia of the external about the wing centre of gravity, and the moment of inertia associated with the wing itself, such that

$$T = \frac{m}{2}\int_0^s \int_0^c \dot{z}^2 dxdy + \frac{m_{ex}}{2}\dot{z}_{ex}^2 + \frac{I_w}{2}\dot{\theta}^2 + \frac{I_{ex}}{2}\dot{\theta}_{ex}^2 \tag{7}$$

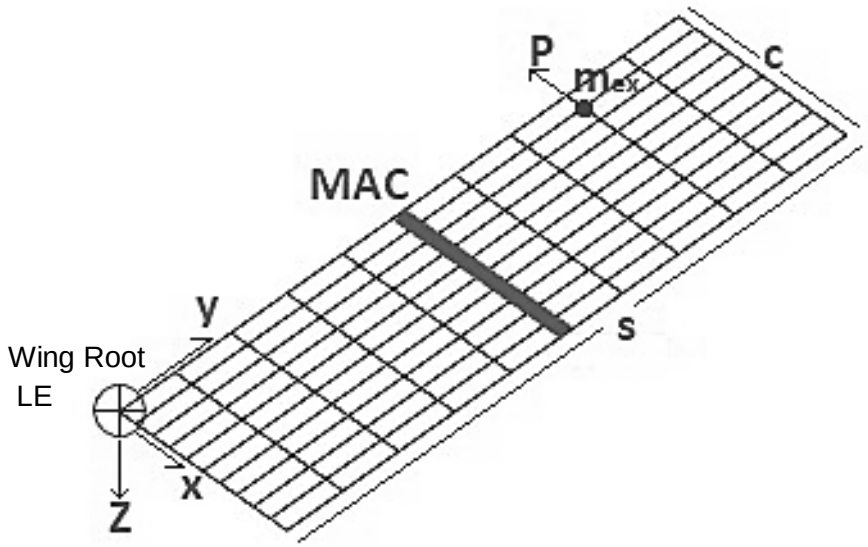

Figure 4-Wing and External Store Layout

The potential energy of the system is due purely to the strain energy effect over the total length of the wing. The external store mass does not contribute to this potential energy

$$U = \frac{1}{2}\int_0^s EI\left(\frac{d^2z}{dy^2}\right)^2 dy + \frac{1}{2}\int_0^s GJ\left(\frac{d^2\theta}{dy^2}\right)^2 dy \tag{8}$$

The approach used for the aerodynamics model is a combination of the simplified Theodorsen method with aerodynamic strip theory [37]. This approach makes use unsteady aerodynamic derivative $M_{\dot{\theta}}$ for

the inclusion of pitch damping crucial for aeroelastic analysis. The lift and moment for each strip dy is given below and can be integrated over the whole wing to give the total lift and moment. As $M_{\dot{\theta}}$ is assumed to be constant, this model is independent of the reduced frequency.

$$dL = \frac{1}{2}\rho V^2 c a_w \left(\frac{\dot{Z}}{V} + \theta\right) dy \tag{9}$$

$$dM = \frac{1}{2}\rho V^2 c^2 \left[e a_w \left(\frac{\dot{Z}}{V} + \theta\right) + \frac{M_{\dot{\theta}}}{4V}\ \dot{\theta}\right] dy \tag{10}$$

The incremental work done by these aerodynamic forces and moments

$$\delta W_a = \int_{wing} [dL(-y^2 \delta q_1 - y^3 \delta q_2) + dM(y\delta q_3 + y^2 \delta q_4)] \tag{11}$$

The external store thrust acts as a follower-force, thus there is also work done by this force which is to be accounted for. For a given span station, work done by this follower-force P through incremental deflection δz and twist $\delta\theta$

$$\begin{aligned} \delta W_P = -P\ sin(\theta)(\delta z_{ex} + r\sin(\theta + \delta\theta) - \mathrm{r}\sin(\theta)) \\ + P\ cos(\theta)(\mathrm{r}\cos(\theta) - \mathrm{r}\cos(\theta + \delta\theta)) \\ \delta W_P = -P\theta\delta z_{ex} \end{aligned} \tag{12}$$

The generalised forces are given with the addition of the incremental word done by the aerodynamic forces and the follower-force of the external store

$$\begin{aligned} Q_{q1} &= \frac{\partial}{\partial}\frac{\delta W_a}{\delta q_1} + \frac{\partial}{\partial}\frac{\delta W_P}{\delta q_1} \\ Q_{q2} &= \frac{\partial}{\partial}\frac{\delta W_a}{\delta q_1} + \frac{\partial}{\partial}\frac{\delta W_P}{\delta q_2} \\ Q_{q3} &= \frac{\partial}{\partial}\frac{\delta W_a}{\delta q_1} + \frac{\partial}{\partial}\frac{\delta W_P}{\delta q_3} \\ Q_{q4} &= \frac{\partial}{\partial}\frac{\delta W_a}{\delta q_1} + \frac{\partial}{\partial}\frac{\delta W_P}{\delta q_4} \end{aligned} \tag{13}$$

A wing of uniform mass distribution has the mass axis fixed along the mid-chord. In order to be able to move the position of the mass axis along the chord, the mass distribution is made to vary linearly from leading to trailing edge, depending on the required mass axis position x_m, as seen in Figure 5.

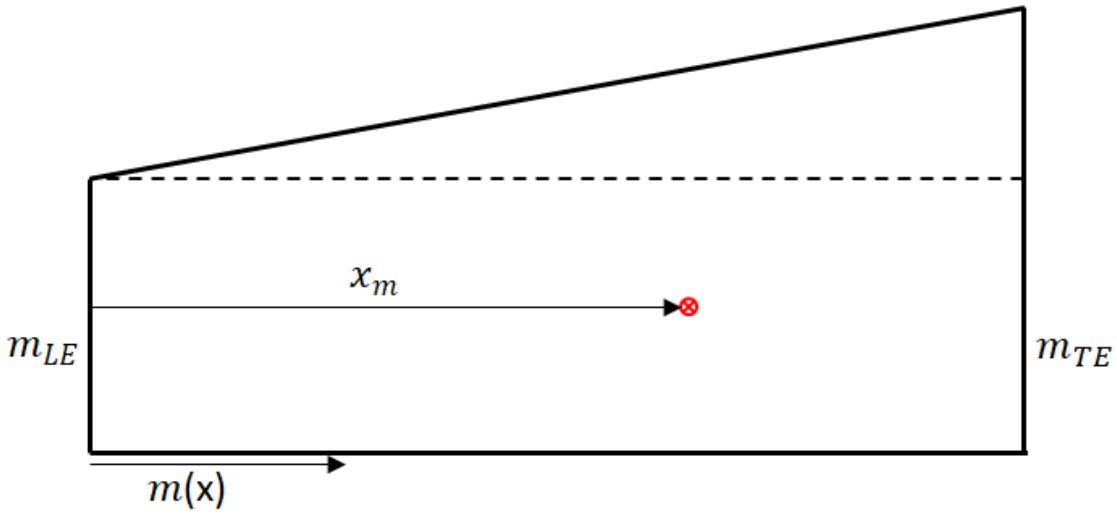

Figure 5-Chord-wise Mass Distribution to Achieve Modified Mass Axis Position

The linear variation of the mass in the x direction can be represented as

$$m(x) = a + bx \tag{14}$$

Where the constants a and b act as weights to adjust the model to achieve the required mass axis position. Equating the area of the original uniform mass chord to that of the modified mass axis chord gives

$$\begin{gathered} m_{TE}c + \frac{c(m_{LE} - m_{TE})}{2} = mc \\ \rightarrow \ (m_{LE} + m_{TE}) = 2m \end{gathered} \tag{15}$$

Equating the moments of the modified mass axis chord to the component parts leads to

$$mx_m = \frac{c^2}{2}m_{LE} + (m_{TE} - m_{LE})\frac{c^2}{3} = \frac{c}{6}(m_{LE} + 2m_{TE}) \tag{16}$$

and this equation can be used to derive the required expressions for m_{LE} and m_{TE}

$$m_{LE} = 2m\left(2 - \frac{3x_m}{c}\right) \tag{17}$$

$$m_{TE} = 2m\left(\frac{3x_m}{c} - 1\right) \tag{18}$$

The values of a and b can been be found by noting that

$$m(x) = a + bx$$
$$a = m_{LE} \quad and \quad b = \left(\frac{m_{TE} - m_{LE}}{c}\right) \tag{19}$$

3.2. Aeroelastic Equation

Returning to Lagrange's equation, the full general aeroelastic equations of motion is now put together in matrix form using the above expressions to achieve the well-known aeroelastic equation, with terms added to account for the external store, with the following terms:

$$(\boldsymbol{A} + \boldsymbol{A_{ex}})\underline{\ddot{\boldsymbol{q}}} + (\rho V \boldsymbol{B})\underline{\dot{\boldsymbol{q}}} + (\rho V^2 \boldsymbol{C} + (\boldsymbol{E} + \boldsymbol{E_{ex}}))\underline{\boldsymbol{q}} = \underline{\boldsymbol{0}} \tag{20}$$

Inertial matrices:

$$\boldsymbol{A} = \begin{bmatrix} A_{11} & A_{12} & A_{13} & A_{14} \\ A_{21} & A_{22} & A_{23} & A_{24} \\ A_{31} & A_{32} & A_{33} & A_{34} \\ A_{41} & A_{42} & A_{43} & A_{44} \end{bmatrix}$$

$$A_{11} = as^5\frac{c}{5} + bs^5\frac{c^2}{10}$$

$$A_{12} = as^6\frac{c}{6} + bs^6\frac{c^2}{12}$$

$$A_{13} = a\frac{s^4}{4}\left(\frac{c^2}{2} - cx_f\right) + b\frac{s^4}{4}\left(\frac{c^3}{3} - c^2\frac{xf}{2}\right)$$

$$A_{14} = a\frac{s^5}{5}\left(\frac{c^2}{2} - cx_f\right) + b\frac{s^5}{5}\left(\frac{c^3}{3} - c^2\frac{x_f}{2}\right)$$

$$A_{21} = as^6\frac{c}{6} + bs^6\frac{c^2}{12}$$

$$A_{22} = as^7\frac{c}{7} + bs^7\frac{c^2}{14}$$

$$A_{23} = a\frac{s^5}{5}\left(\frac{c^2}{2} - cx_f\right) + b\frac{s^5}{5}\left(\frac{c^3}{3} - c^2\frac{x_f}{2}\right)$$

$$A_{24} = a\frac{s^6}{6}\left(\frac{c^2}{2} - cx_f\right) + b\frac{s^6}{6}\left(\frac{c^3}{3} - c^2\frac{x_f}{2}\right)$$

$$A_{31} = a\frac{s^4}{4}\left(\frac{c^2}{2} - cx_f\right) + b\frac{s^4}{4}\left(\frac{c^3}{3} - c^2\frac{x_f}{2}\right)$$

$$A_{32} = a\frac{s^5}{5}\left(\frac{c^2}{2} - cx_f\right) + b\frac{s^5}{5}\left(\frac{c^3}{3} - c^2\frac{x_f}{2}\right)$$

$$A_{33} = a\frac{s^3}{3}\left(\frac{c^3}{3} - c^2x_f + cx_f^2\right) + b\frac{s^3}{3}\left(\frac{c^4}{4} - 2c^3\frac{x_f}{3} + c^2\frac{x_f^2}{2}\right) + I_w\frac{s^3}{3}\left(\frac{c^3}{3} - c^2x_f + cx_f^2\right)$$

$$A_{34} = a\frac{s^4}{4}\left(\frac{c^3}{3} - c^2x_f + cx_f^2\right) + b\frac{s^4}{4}\left(\frac{c^5}{5} - c^4\frac{x_f}{2} + c^3\frac{x_f^2}{3}\right) + I_w\frac{s^4}{4}\left(\frac{c^3}{3} - c^2x_f + cx_f^2\right)$$

$$A_{41} = a\frac{s^5}{5}\left(\frac{c^2}{2} - cx_f\right) + b\frac{s^5}{5}\left(\frac{c^3}{3} - c^2\frac{x_f}{2}\right)$$

$$A_{42} = a\frac{s^6}{6}\left(\frac{c^2}{2} - cx_f\right) + b\frac{s^6}{6}\left(\frac{c^3}{3} - c^2\frac{x_f}{2}\right)$$

$$A_{43} = a\frac{s^4}{4}\left(\frac{c^3}{3} - c^2x_f + cx_f^2\right) + b\frac{s^4}{4}\left(\frac{c^5}{5} - c^4\frac{x_f}{2} + c^3\frac{x_f^2}{3}\right) + I_w\frac{s^4}{4}\left(\frac{c^3}{3} - c^2x_f + cx_f^2\right)$$

$$A_{44} = a\frac{s^5}{5}\left(\frac{c^3}{3} - c^2xf + cx_f^2\right) + b\frac{s^5}{5}\left(\frac{c^4}{4} - 2c^3\frac{xf}{3} + c^2\frac{xf^2}{2}\right) + I_w\frac{s^5}{5}\left(\frac{c^3}{3} - c^2x_f + cx_f^2\right)$$

$$\boldsymbol{A_{ex}} = \begin{bmatrix} A_{ex11} & A_{ex12} & A_{ex13} & A_{ex14} \\ A_{ex21} & A_{ex22} & A_{ex23} & A_{ex24} \\ A_{ex31} & A_{ex32} & A_{ex33} & A_{ex34} \\ A_{ex41} & A_{ex42} & A_{ex43} & A_{ex44} \end{bmatrix}$$

$$A_{ex11} = m_{ex}y_{ex}^4$$

$$A_{ex12} = m_{ex}y_{ex}^5$$

$$A_{ex13} = m_{ex}y_{ex}^3(x_{ex} - x_f)$$

$$A_{ex14} = m_{ex}y_{ex}^4(x_{ex} - x_f)$$

$$A_{ex21} = m_{ex}y_{ex}^5$$

$$A_{ex22} = m_{ex}y_{ex}^6$$

$$A_{ex23} = m_{ex}y_{ex}^4(x_{ex} - x_f)$$

$$A_{ex24} = m_{ex}y_{ex}^5(x_{ex} - x_f)$$

$$A_{ex31} = m_{ex} y_{ex}^3 (x_{ex} - x_f)$$

$$A_{ex32} = m_{ex} y_{ex}^4 (x_{ex} - x_f)$$

$$A_{ex33} = m_{ex} y_{ex}^2 (x_{ex} - x_f)^2 + I_{ex} y_{ex}^2 (x_{ex} - x_f)^2$$

$$A_{\mathrm{ex34}} = m_{ex} y_{ex}^3 (x_{ex} - x_f)^2 + I_{ex} y_{ex}^3 (x_{ex} - x_f)^2$$

$$A_{ex41} = m_{ex} y_{ex}^4 (x_{ex} - x_f)$$

$$A_{ex42} = m_{ex} y_{ex}^5 (x_{ex} - x_f)$$

$$A_{ex43} = m_{ex} y_{ex}^3 (x_{ex} - x_f)^2 + I_{ex} y_{ex}^3 (x_{ex} - x_f)^2$$

$$A_{ex44} = m_{ex} y_{ex}^4 (x_{ex} - x_f)^2 + I_{ex} y_{ex}^4 (x_{ex} - x_f)^2$$

Aerodynamic damping matrix:

$$\boldsymbol{B} = \begin{bmatrix} ca_w \frac{s^5}{10} & ca_w \frac{s^6}{12} & 0 & 0 \\ ca_w \frac{s^6}{12} & ca_w \frac{s^7}{14} & 0 & 0 \\ -c^2 e a_w \frac{s^4}{8} & -c^2 e a_w \frac{s^5}{10} & -c^3 M_{\dot{\theta}} \frac{s^3}{24} & -c^3 M_{\dot{\theta}} \frac{s^4}{32} \\ -c^2 e a_w \frac{s^5}{10} & -c^2 e a_w \frac{s^6}{12} & -c^3 M_{\dot{\theta}} \frac{s^4}{32} & -c^3 M_{\dot{\theta}} \frac{s^5}{40} \end{bmatrix}$$

Aerodynamic stiffness matrix:

$$\boldsymbol{C} = \begin{bmatrix} 0 & 0 & ca_w \frac{s^4}{8} & ca_w \frac{s^5}{10} \\ 0 & 0 & ca_w \frac{s^5}{10} & ca_w \frac{s^6}{12} \\ 0 & 0 & -c^2 e a_w \frac{s^3}{6} & -c^2 e a_w \frac{s^4}{8} \\ 0 & 0 & -c^2 e a_w \frac{s^4}{8} & -c^2 e a_w \frac{s^5}{10} \end{bmatrix}$$

Structural stiffness matrices:

$$\boldsymbol{E} = \begin{bmatrix} 4EIs & 6s^2EI & 0 & 0 \\ 6s^2EI & 12s^3EI & 0 & 0 \\ 0 & 0 & GJs & GJs^2 \\ 0 & 0 & GJs^2 & \frac{4}{3}GJs^3 \end{bmatrix}$$

$$\boldsymbol{E_{ex}} = \begin{bmatrix} 0 & 0 & Py_{ex}^3 & Py_{ex}^4 \\ 0 & 0 & Py_{ex}^4 & Py_{ex}^5 \\ 0 & 0 & Py_{ex}^2(x_{ex} - x_f) & Py_{ex}^3(x_{ex} - x_f) \\ 0 & 0 & Py_{ex}^3(x_{ex} - x_f) & Py_{ex}^4(x_{ex} - x_f) \end{bmatrix}$$

As was done with the inertial matrix, the structural matrix is separated for the terms relating to the wing itself and terms relating the external follower-force. There are no terms for the inclusion of structural damping which has been ignored. The systems frequencies and damping ratios can be determined by taking the eigenvalue solution of the aeroelastic equation of motion

$$\begin{Bmatrix} \dot{\underline{q}} \\ \ddot{\underline{q}} \end{Bmatrix} - \begin{bmatrix} \boldsymbol{0} & \boldsymbol{I} \\ -(\boldsymbol{A} + \boldsymbol{A_{ex}})^{-1}(\rho V^2 \boldsymbol{C} + \boldsymbol{E} + \boldsymbol{E_{ex}}) & -(\boldsymbol{A} + \boldsymbol{A_{ex}})^{-1}(\rho V \boldsymbol{B}) \end{bmatrix} \begin{Bmatrix} \underline{\boldsymbol{q}} \\ \dot{\underline{\boldsymbol{q}}} \end{Bmatrix} = \underline{\boldsymbol{0}} \tag{21}$$

It is noted that although the stiffness matrices contain high order terms, these cancel out when divided by the inertial matrices. The equation now takes the standard eigen problem form

$$\dot{\boldsymbol{x}} - \boldsymbol{Q}\boldsymbol{x} = \boldsymbol{0} \tag{22}$$

With the eigenvalues of system matrix $\boldsymbol{Q}$ occurring in conjugate pairs for oscillatory poles

$$\lambda_j = -\zeta_j \omega_j \pm j\omega_j \sqrt{1 - \zeta_j^2}, \quad j = 1, 2, \dots, N$$

3.3. Gust Expressions

In order to compute the gust response of the wing/store system, the aeroelastic equation needs to be modified to include a gust input expression. The gust term is incorporated into the aerodynamic expressions as shown below

$$dL = \frac{1}{2}\rho V^2 c a_w \left(\frac{\dot{Z}}{V} + \theta + \frac{\omega_g}{V}\right) dy \tag{23}$$

$$dM = \frac{1}{2}\rho V^2 c^2 \left[e a_w \left(\frac{\dot{Z}}{V} + \theta\right) + \frac{M_{\dot{\theta}}}{4V}\,\dot{\theta} + \frac{\omega_g}{V}\right] dy \tag{24}$$

As before, these expressions are used in the aerodynamic work done but with all the terms related to the gust kept on the right hand side of the aeroelastic equation, forming its own column matrix. The aeroelastic equation now allows the response of the wing to a known gust time history to be calculated.

$$(\boldsymbol{A} + \boldsymbol{A_{ex}})\ddot{\underline{\boldsymbol{q}}} + (\rho V \boldsymbol{B})\dot{\underline{\boldsymbol{q}}} + \left(\rho V^2 \boldsymbol{C} + (\boldsymbol{E} + \boldsymbol{E_{ex}})\right)\underline{\boldsymbol{q}} = \boldsymbol{F_{gust}} = \rho V c a_w \begin{bmatrix} -\frac{s^3}{6} \\ -\frac{s^4}{8} \\ \frac{ces^2}{4} \\ \frac{ces^3}{6} \end{bmatrix} \omega_g(t) \tag{25}$$

The type of gust input investigated in this thesis is a family of 1-cosine gusts taking the form [37]

$$\omega_g(t) = \frac{U_{ds}}{2}\left(1 - \cos\left(\frac{2\pi V}{L_g} t\right)\right) \tag{26}$$

The maximum value of a given 1-cosine gust, or the design gust velocity, U_{ds} is given in terms of the gust wavelength, H and a reference gust velocity in the following expression [37]

$$U_{ds} = U_{ref}\left(\frac{H}{107}\right)^{\frac{1}{6}} \tag{27}$$

In this analysis, the reference velocity U_{ref} is taken as a constant at 17.07 m/s which is the largest value that occurs at sea level. The gust half wavelengths are investigated between 9m to 107m as per the airworthiness regulations [37]. These regulations regulate how the various gust magnitudes and durations correspond to different aircraft sizes and flight conditions, and so an assumption has been made on the size of the aircraft.

4. Flutter Results

As stated in section 3, two bending modes and two torsional modes are considered in the Lagrangian equations of motion. The analyses method presented above was applied to a straight rectangular wing with the properties presented in table 2. To clarify the effect of the external store, the results are presented in the form of three dimensional mesh plots showing how the flutter or divergence speed varies as the extremal store is moved span-wise and chord-wise. Results are presented in three categories. Firstly, the external store takes the form of a point mass. Secondly, the external store follower-force acting at a single point. Finally, the results are shown for both point mass and follower-force present simultaneously.

Table 2 - System Geometry, Aerodynamic, and Material Properties[10]	
s	6.1 (m)
c	1.8 (m)
m	19.53 (Kg/m^2)
ρ	1.02 (Kg/m^3)
a_w	5.73 (1/rad)
$M_{\dot{\theta}}$	-1.2 (N.m)
EI	9.77e+6 (N.m^2)
GJ	0.99e+6 (N.m^2/rad)
x_m	43%.c
x_f	33%.c

Each subsection presents three figures for incrementally increased external mass and/or follower force magnitude. The values of external mass and follower-force magnitudes range from 5% to 15% wing mass and 500% to 1500% wing weight respectively. Following an analysis of civil aircraft, it was found these magnitudes for external mass are relatively small, but relatively high for the external follower-force. The reason for this choice in mass and follower-force range was that higher values for mass make the results less clear, whereas smaller values of follower-force do not affect the flutter speed enough. This external store is moved along the wing and the flutter speed calculated at each station which is then presented as a mesh plot.

From figures 5 to 13 two plots are shown. The top plot shows the flutter or divergence speed depending on which is reached first. The lower plot maps out the flutter frequency and how this varies with the external store position. Positions where the mode frequency is zero indicates there is no oscillation in the mode. For these positions, and as the real parts of the roots are positive the system is experiencing divergence.

4.1. Validation of Flutter Model

Selection of the Goland wing for analysis lends itself to the additional benefit of easy model validation. Other works have used the Goland wing to compare their results. Table 3 compares the flutter speed derived through the exact differentiation of the equations of motion by Goland & Luke [13]. The results compared show a reasonably good correlation of the present predicted flutter speed and frequency to the previous results of other work. The flutter speed and frequency have been calculated by eigenvalue analysis of the governing equation.

Table 3-Validation of Flutter Speed and Frequency for Clean Wing Configuration[23]

Method	**Flutter Speed (m/s)**	**Error (%)**	**Flutter Frequency (Hz)**	**Error (%)**
Goland & Luke[13] (Exact)	137.3	_	11.25	_
Housner and Stein[38]	134.2	-2.26	11.27	0.18
Gern & Librescu[27]	137.1	-0.15	12.02	6.84
Patil and Hodges[39]	135.6	-1.24	11.17	-0.71
Qin and Librescu[40]	137.0	-0.22	11.15	-0.89
Fazelzadeh et al[41]	137.1	-0.15	12.02	6.84
Mazidi & Fazelzadeh[23]	136.9	0.29	11.34	0.80
This Thesis	144.0	4.88	11.45	1.78

4.2. Wing with Point Mass

This first subsection presents the effects of external point mass only on the instability speeds and how this speed varies with such mass. The effects of an external point mass 5% of the mass of the wing can be seen in figure 6. Firstly, it is noted that when placed along the wing root, the resulting flutter speed is that of clean wing configuration at 144 m/s and a flutter frequency of 11.45 Hz. As the mass is moved span-wise away from the root the flutter speed initially drops slightly but recovers as the mid-span is reached. From here, flutter speed increases moderately above the clean wing flutter speed. These variations are more pronounced at the leading and trailing edge. Very little change is seen in the

flutter frequency up to the 80% span. Towards the wing-tip, a transition is seen where the flutter speed becomes more dependent on the chord-wise placement of the mass apart from around the mid-chord of the wing-tip where very little change takes place. At the trailing edge of the wing, the external mass placement causes a sudden notable drop in the flutter speed and frequency. The flutter frequency at the wing-tip trailing edge has dropped to around 9.64 Hz. The 80-90% chord wing-tip is the critical mass placement position with a flutter speed of 135 m/s. Mass placement around the leading edge of the wing-tip sees a drastic increase in flutter speed and at the final station at the leading edge wing-tip divergence speed is reached indicated by the sudden drop in flutter frequency to zero.

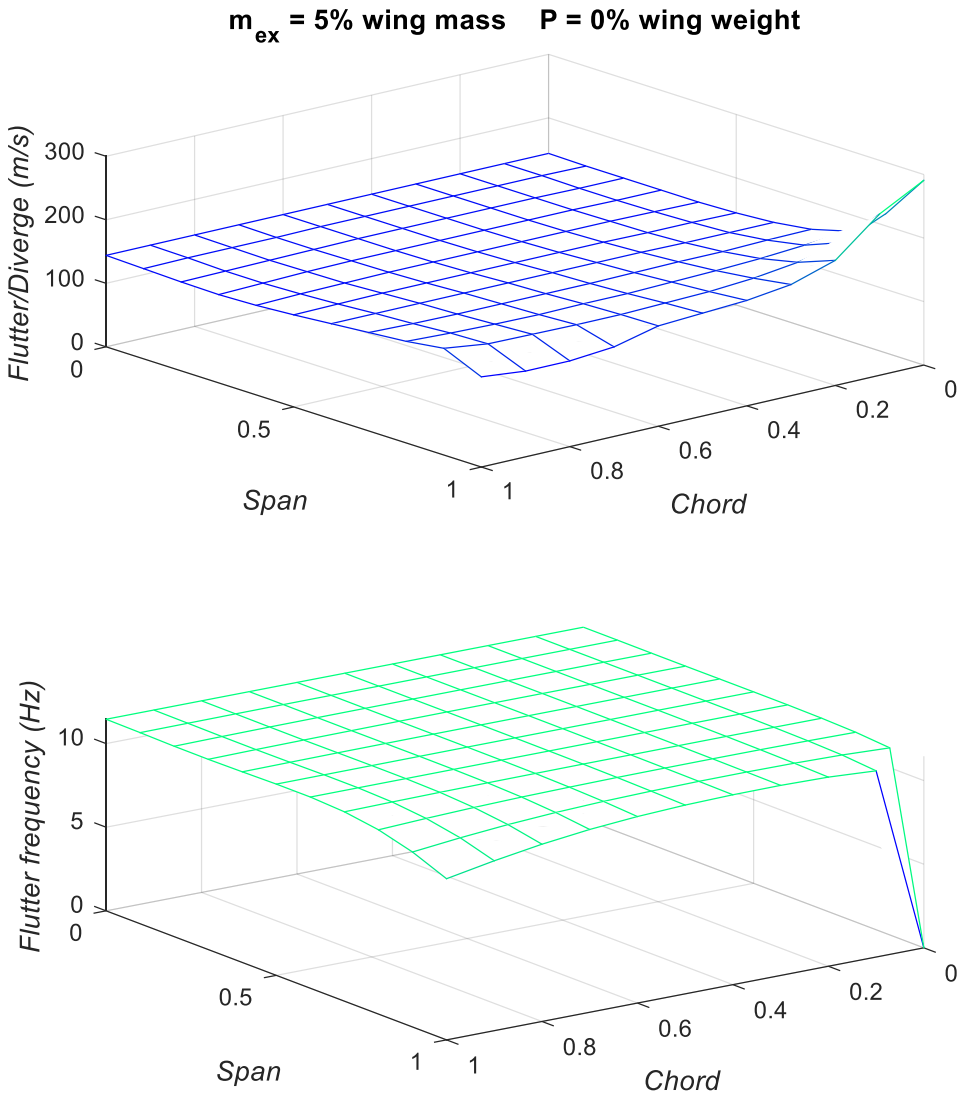

Figure 6-Variation of Flutter/Divergence Speed and Frequency with External Mass Location

In figure 7, an external mass of 10% the mass of the wing is used. Initially there is, again, little change in the flutter speed and frequency as the external mass is moved span-wise away from the wing root where flutter speed is at clean wing conditions. A transition is then seen around the 70% span. Towards the trailing edge of the wing-tip, external mass results in a significant drop in flutter speed and frequency. Flutter frequency at this position drops to its lowest value of 4.6 Hz. If the external mass is moved towards the leading edge again there is a sharp rise to the divergence speed to 291 m/s. The most critical location for mass placement is at the wing-tip 80% chord where the flutter speed is 95 m/s.

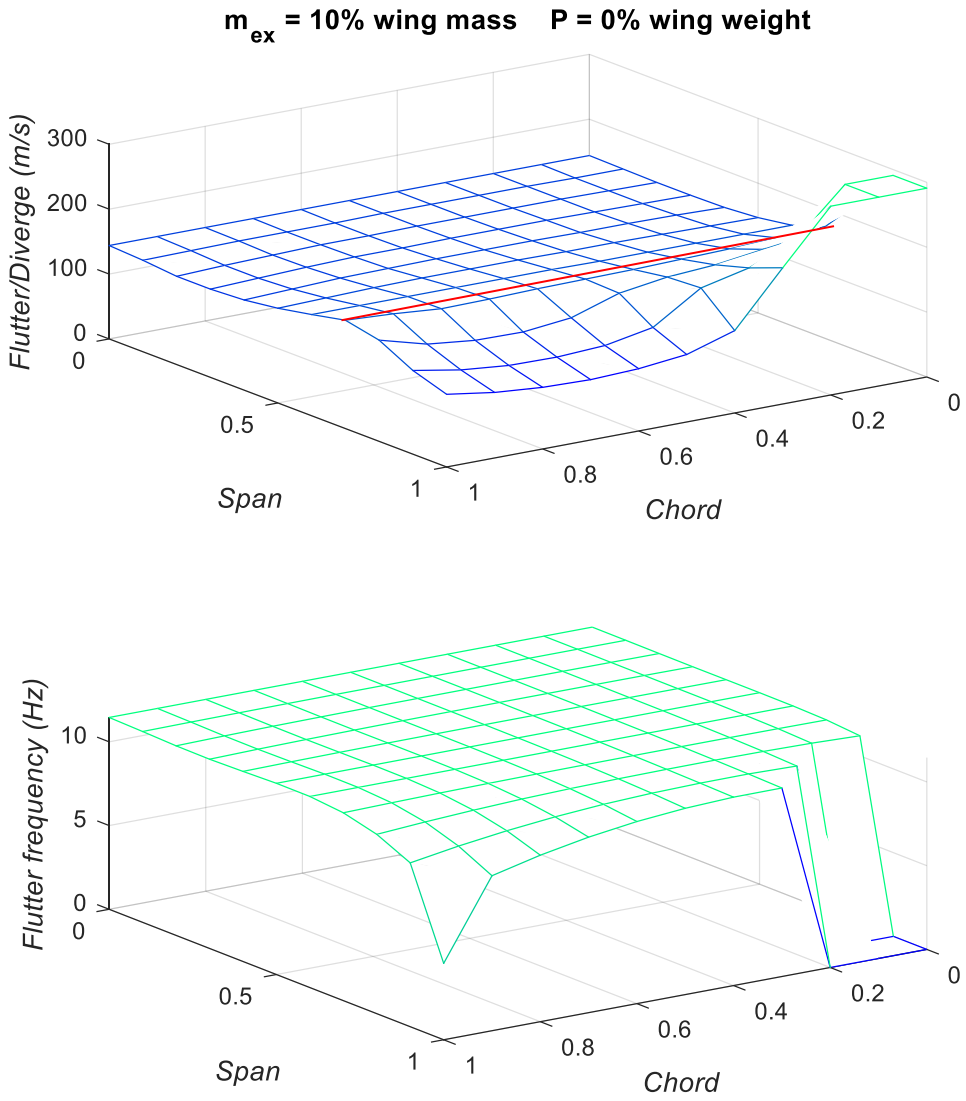

Figure 7-Variation of Flutter/Divergence Speed and Frequency with External Mass Location

Figure 8 shows the effect of the position an external mass 15% the wing mass has. This time a transitional point has moved slightly towards the wing root is reached along the 60% span where flutter speed reaches around 160 m/s. The area of high instability speed around the leading edge wing-tip has expanded further. The critical location for external mass placement is around the wing-tip mid-chord with a flutter speed of 77 m/s, almost half the clean wing flutter speed. The flutter frequency reaches its lowest value of 4.2 Hz at the wing-tip trailing edge.

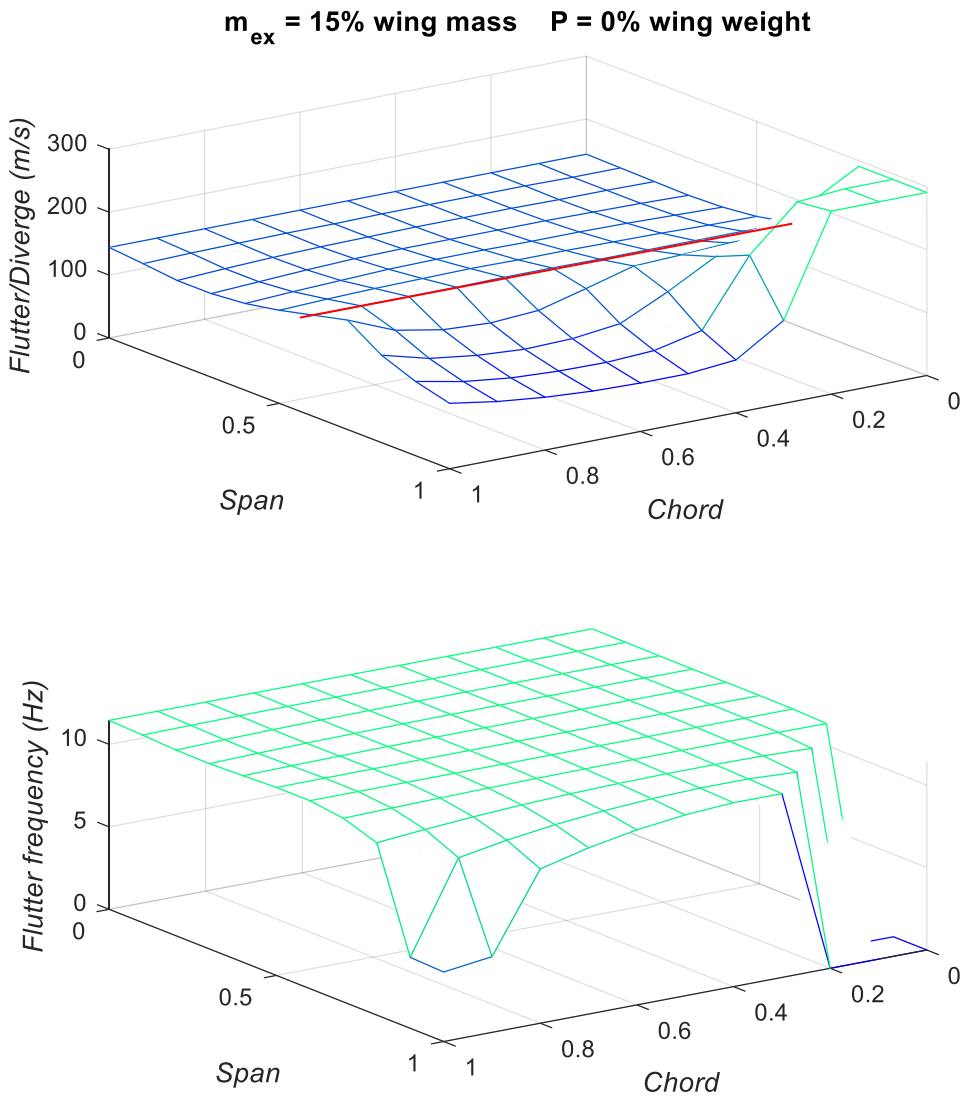

Figure 8-Variation of Flutter/Divergence Speed and Frequency with External Mass Location

4.3. Wing with Follower-Force

With the external mass now set to zero, this subsection looks at the effects of a follower force of increasing magnitude. A follower force of 500% of the weight of the wing is shown in figure 9. As was the case for the external mass, placement of the force along the wing root has no effect and so the flutter speed is that of clean wing configuration.

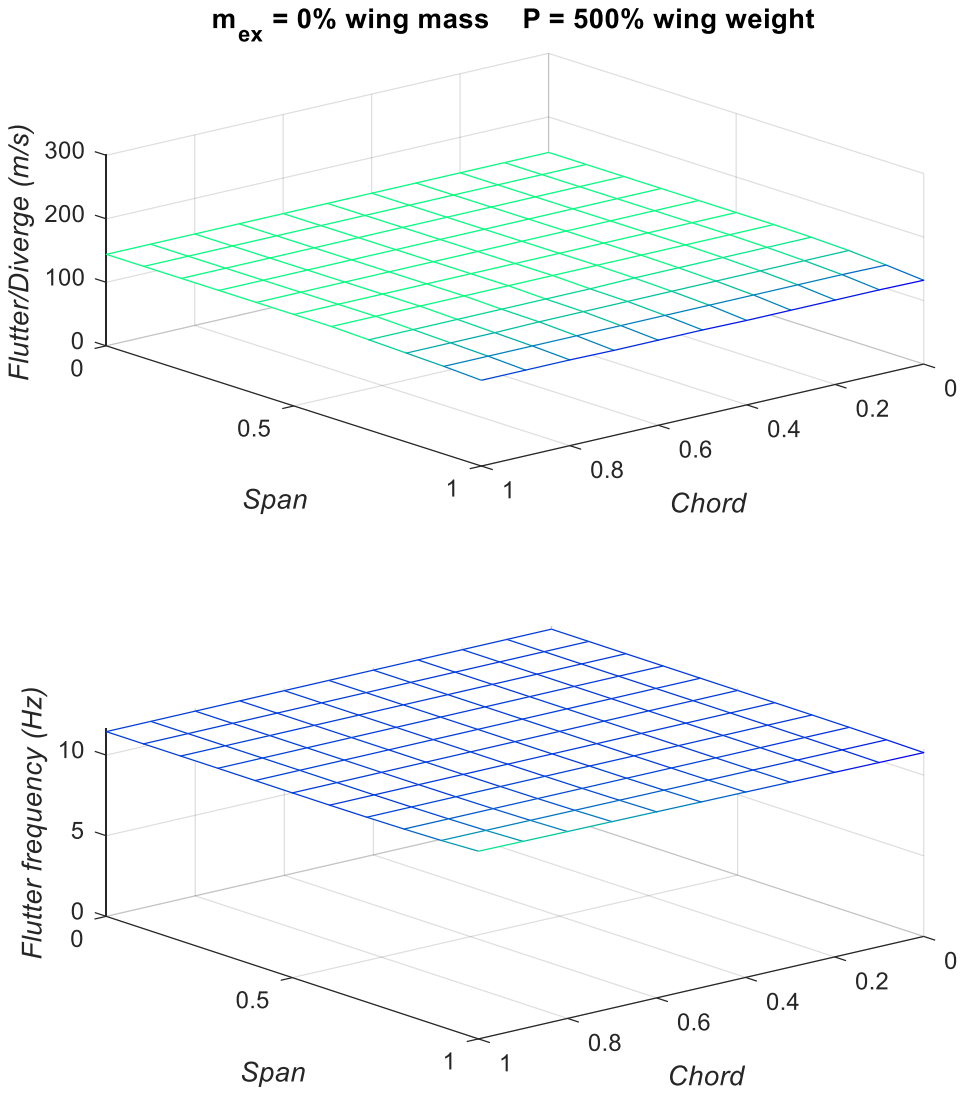

Figure 9-Variation of Flutter/Divergence Speed and Frequency with Follower Force Location

The flutter speed can be seen to vary mainly with span-wise movement of the follower force position. Only very slight decrease in flutter speed is seen as the follower force is moved span-wise until the wing-tip is reached. Along the wing-tip, the leading edge is found to be the critical position with

flutter speed dropping to 132 m/s. The flutter frequency shows negligible change apart from at the wing-tip trailing-edge where flutter frequency increases to above 11.6 Hz, and at the wing-tip leading edge where it drops slightly to 11.4 Hz.

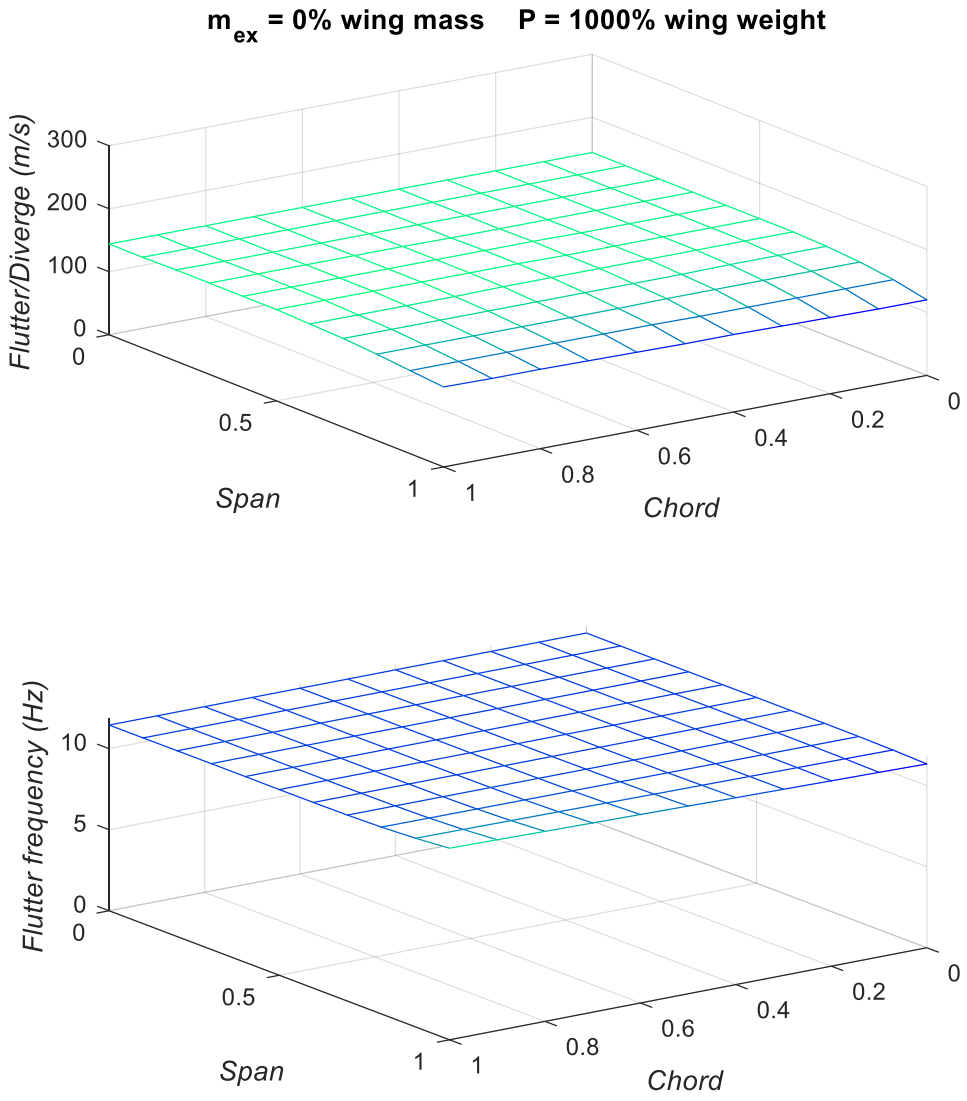

Figure 10-Variation of Flutter/Divergence Speed and Frequency with Follower Force Location

The effects of the position of a wing mounted follower force of magnitude equal to 1000% the weight of the wing is shown in figure 10. This time, a sharper decrease in flutter speed can be seen when the follower force approaches the wing-tip. The critical placement of the follower force is the leading edge of the wing-tip where flutter speed this time drops to 120 m/s. At the trailing edge of the wing-tip

flutter speed drops to 127 m/s, whereas the flutter frequency at this point has increased to above 11.8 Hz.

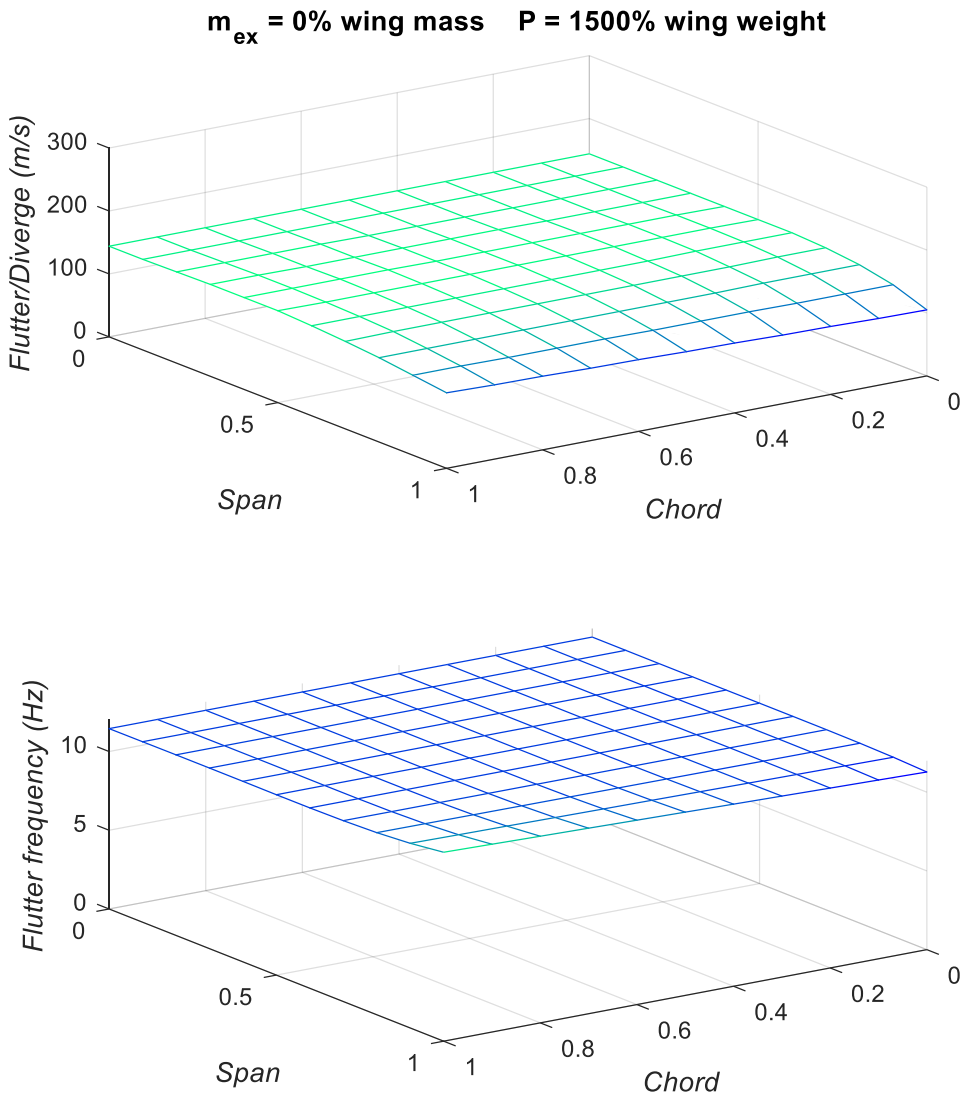

Figure 11-Variation of Flutter/Divergence Speed and Frequency with Follower Force Location

Figure 11 uses the largest follower force magnitude at 1500% wing weight. The flutter speed at the critical location of leading edge wing-tip has this time dropped to 105 m/s and flutter frequency is 11.28 Hz. At the trailing edge of the wing-tip flutter speed decreases to 120 m/s. The flutter frequency at this point has increased to 12 Hz.

4.4. Wing with Follower-Force and Mass

This subsection explores the effects of an external store with properties of both mass and follower force. Generally, these plots take a very similar form as those showing the effects of external mass only but with specific instability speed values slightly altered dues to the follower force. Figure 12 shows the effects of an external store with mass 5% the mass of the wing and follower force 500% the weight of the wing. Similarly to previous plots, along the wing root, flutter speed and frequency is that of clean wing configuration.

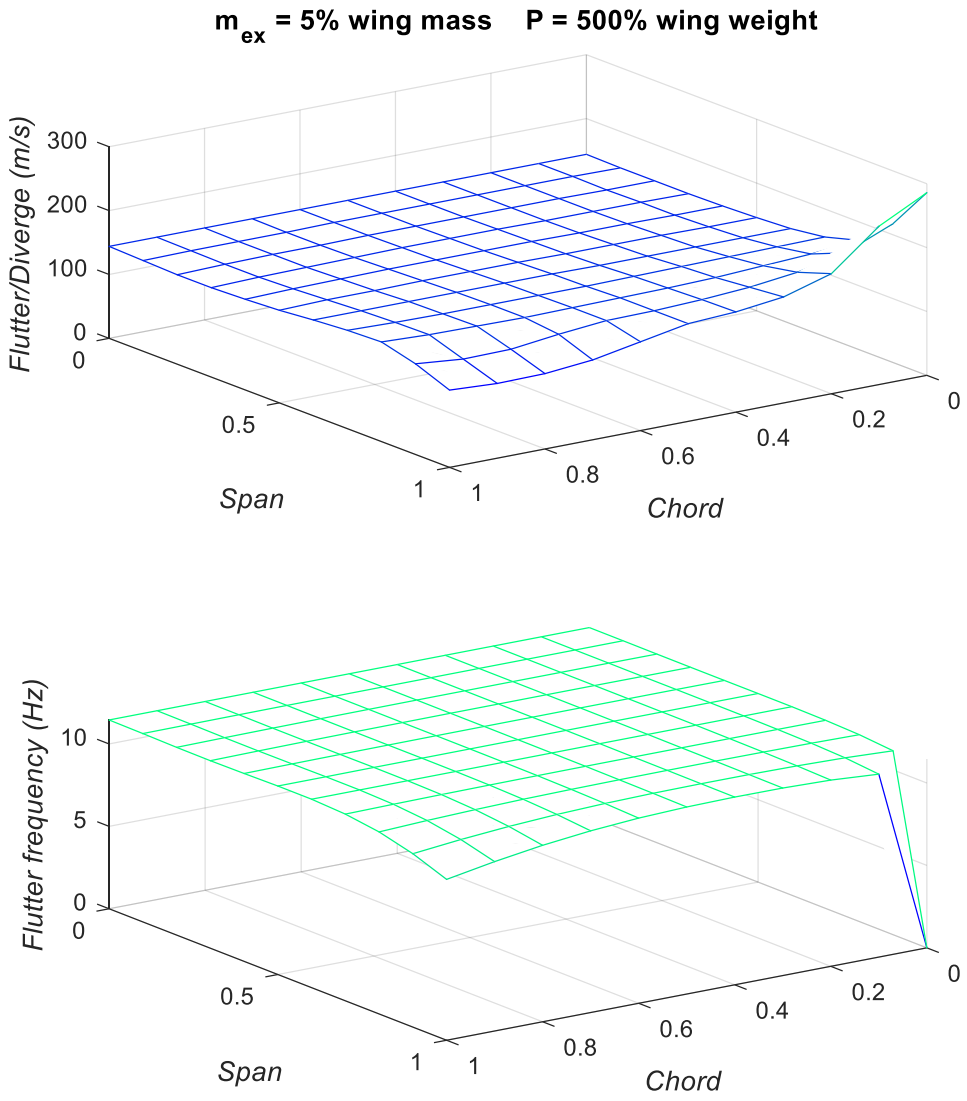

Figure 12-Variation of Flutter/Divergence Speed and Frequency with External Mass and Follower Force Location

At the leading edge wing-tip, the instability is now divergence speed. However, this divergence speed is now 286 m/s, down from 291 m/s for the case of external mass only. The critical position for the mass/thrust is 90% chord of the wing-tip, as it was in figure 6, but with flutters speed notably reduced to 117 m/s from a previous 135 m/s. The flutter frequency at the wing-tip trailing edge is down slightly to 9.64 Hz

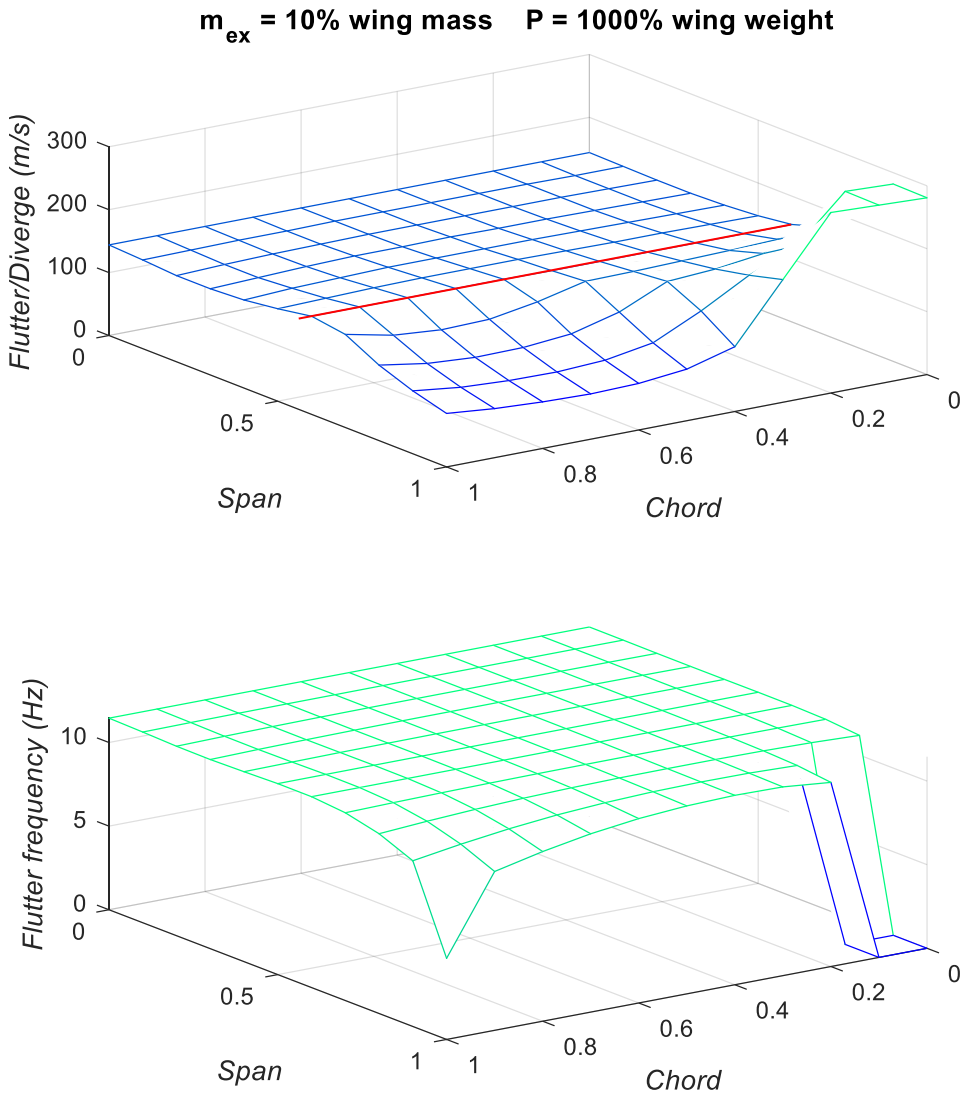

Figure 13-Variation of Flutter/Divergence Speed and Frequency with External Mass and Follower Force Location

The external store in figure 13 has a mass and follower force of 10% wing mass and 1000% wing weight respectively. Along the leading and trailing edge, with span-wise movement of the mass/thrust

away from the wing root, we see an initial drop in flutter speed which then recovers to 156 m/s running along the 60% span where, again, a transition is seen similar to that of the results for external mass only. Notably, this transition point has moved closer to the wing root and the flutter speed is lower than that seen in figure 7. The 70% chord of the wing-tip is the critical position with a flutter speed at this point being 72 m/s, more than 20 m/s lower than that for external mass only. The abrupt drop in flutter frequency at the very trailing edge of the wing-tip is around 8.5 Hz, which is slightly higher compared to mass only. At the leading edge of the wing-tip, divergence speed is reached at multiple stations.

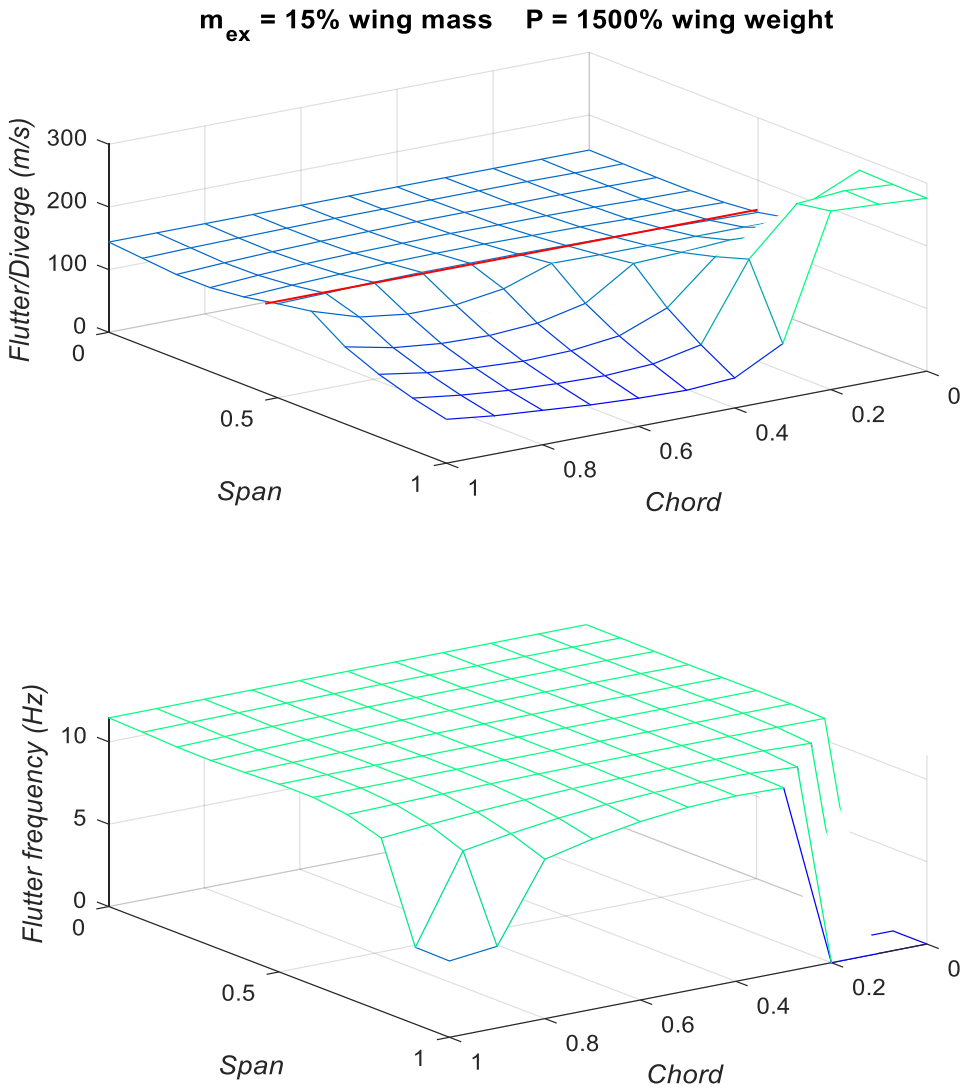

Figure 14-Variation of Flutter/Divergence Speed and Frequency with External Mass and Follower Force Location

The effects of external store location with a mass 15% the wing weight and thrust 1500% of the weight of the wing is presented in figure 14. The critical external store position is now at the mid-chord of the wing-tip where the flutter speed reaches as low as 43 m/s. The transition point is also running directly along the mid-span with flutter speed hovering just above 150 m/s. Divergence speed is reached at the leading edge of the wing-tip. The flutter frequency at the very trailing edge of the wing-tip is around 4.6 Hz. This finding is again higher compared to that of the 15% mass only case which was roughly 4.2 Hz. The flutter frequency in general falls at a very slow rate as the external store is moved span-wise from the root, with usual exception of the leading and trailing edge of the wing-tip, which see far more drastic changes.

4.5. Mass vs Follower Force Plots

This section presents plots showing how the instability speed varies with mass vs thrust or follower force providing a good summery of such effects. Given that external stores have been seen to cause the most interesting effects at the leading and trailing edge of the wing-tip, plots are shown close to these two points. Instability speed can take the form of flutter or divergence.

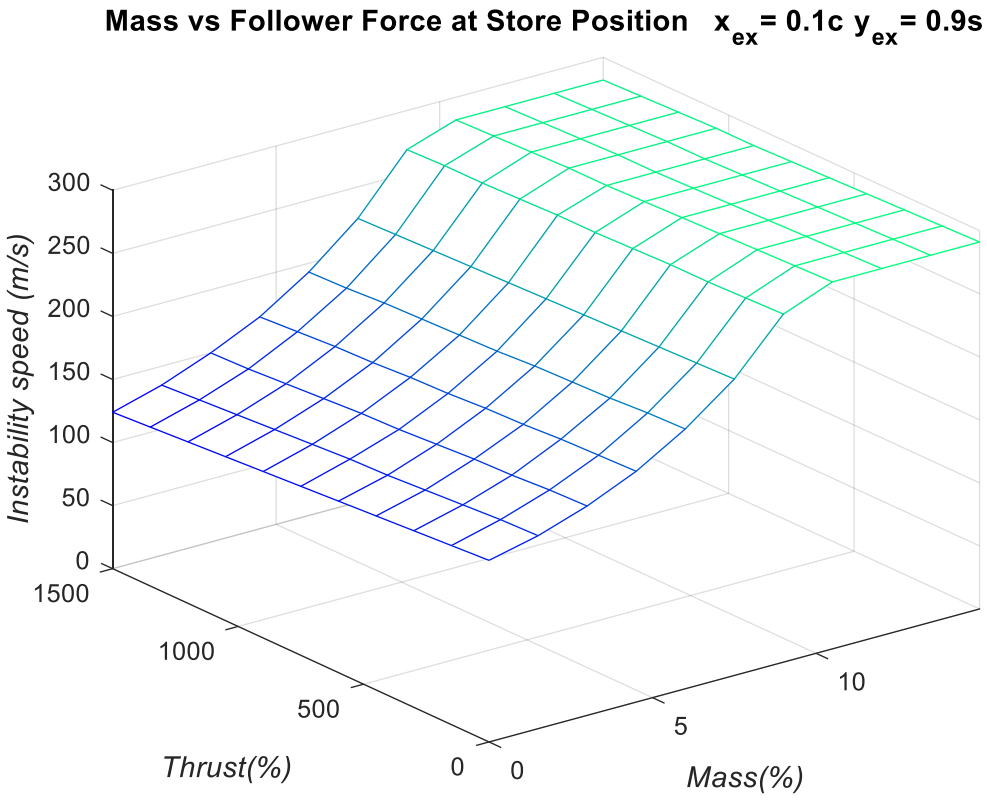

Figure 15 External Mass vs Thrust Near to Leading Edge Wing-tip

Figure 15 plots how the instability speed varies for a range of mass and thrust values at a station on the wing located at the 10% chord / 90% span position. For any given amount of mass, change in instability is reduced marginally with thrust. Instability speed changes most drastically along the mass axis. Instability speed is seen to increase exponentially with mass up to a magnitude of 10% mass. Increasing mass beyond this cause no change in instability speed. However, the instability still varies with thrust at these high external mass percentages.

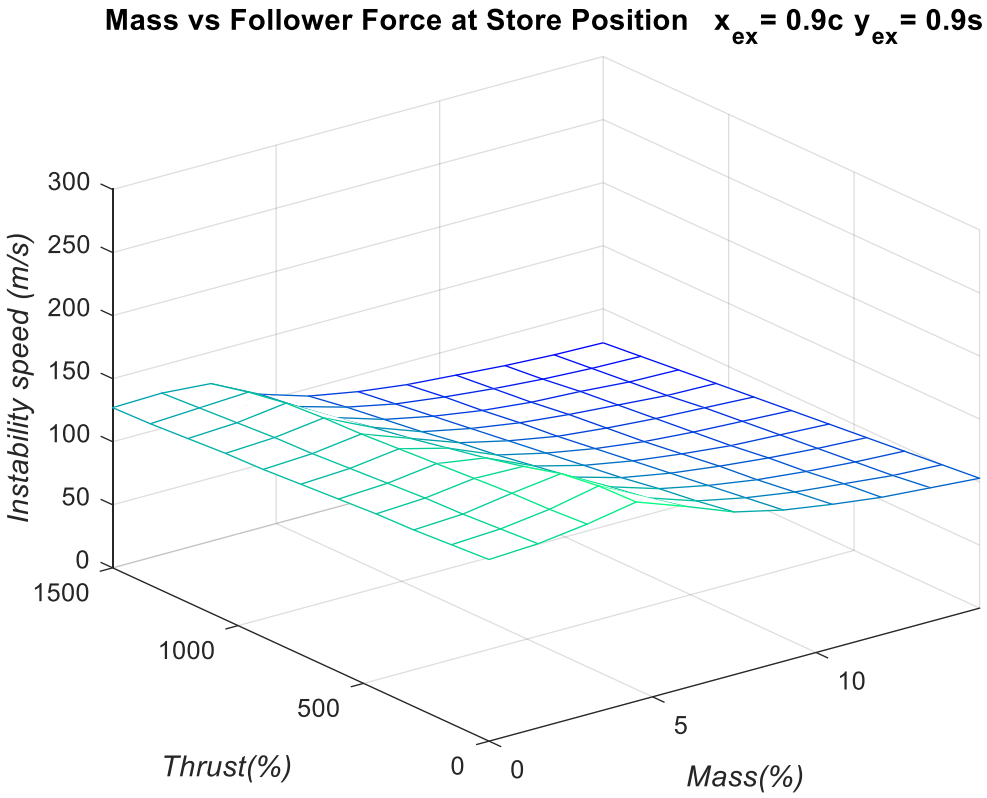

Figure 16-External Mass vs Thrust Near to Trailing Edge Wing-tip

Figure 16 plots how instability speed changes for a range of external mass and thrust at a point at the 90% chord / 90% span. In contrast to figure 15, the increasing mass is seen to generally decrease the instability speed. Initially, increasing mass increases instability speed up to mass values of 4% for low thrust values and 3% for high thrust values. Increasing mass beyond this steadily decreases instability speed. Again, increasing the thrust causes a marginal decrease in instability speed.

4.6. Variation in Mode Frequencies

This section presents results showing how each of the mode frequencies varies with external store configuration and position. The positions of the external store investigated are summarised in table 4.

The mass and follower-force varied from 0-15% wing mass and 0-1500% wing weight respectfully. The four modes are ranked in order of frequency from lowest to highest.

Table 4-External Store Positions		
Point	**Span Position**	**Chord Position**
1	50% (Mid)	0% (LE)
2	100% (Tip)	0% (LE)
3	50% (Mid)	100% (TE)
4	100% (Tip)	100% (TE)

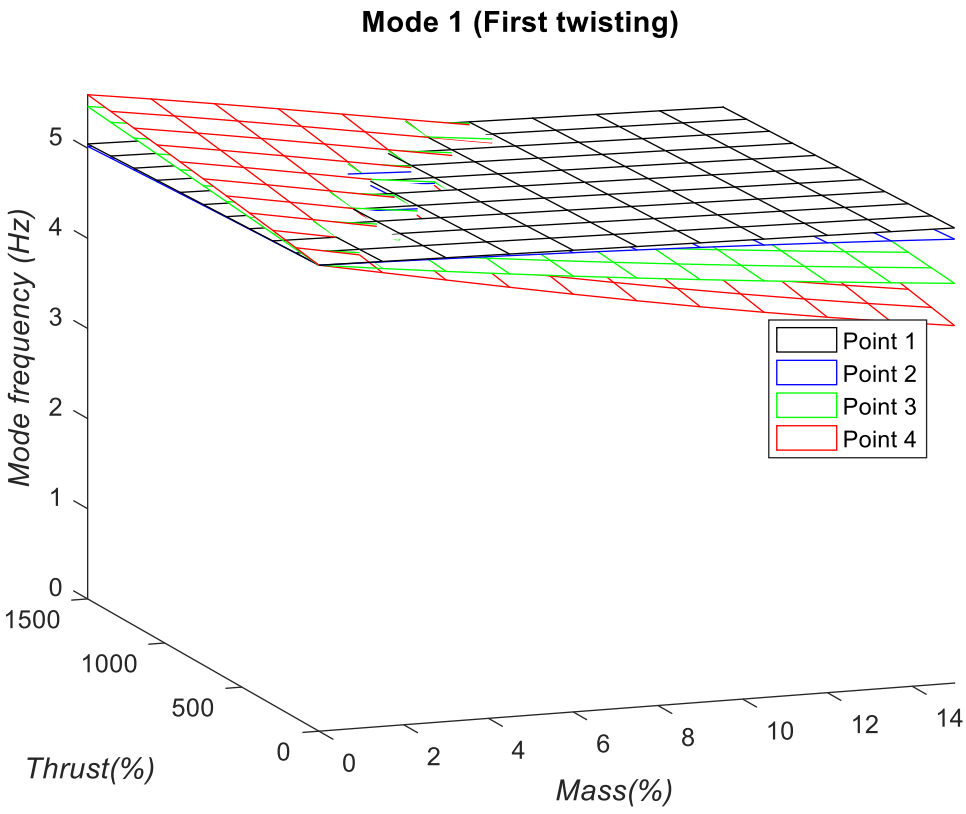

Figure 17-Mode 1 Frequency Variation with External Store Configuration and Position

Figure 17 shows how the frequency of the first twisting mode varies with external store mass, thrust, and position on the wing. Each surface represents a different position on the wing. As expected, the surfaces converge as the external mass and trust reduce to zero to give the modes frequency of

5.169Hz for clean wing configuration. For point 1 and 2, both located at the leading edge but a half span apart, very little variance is seen with either external mass or thrust. Point 3 and 4, located along the trailing edge; see a variation with both external mass and thrust. Application of the external mass causes a reduction in mode frequency at these two points whereas the thrust increases it.

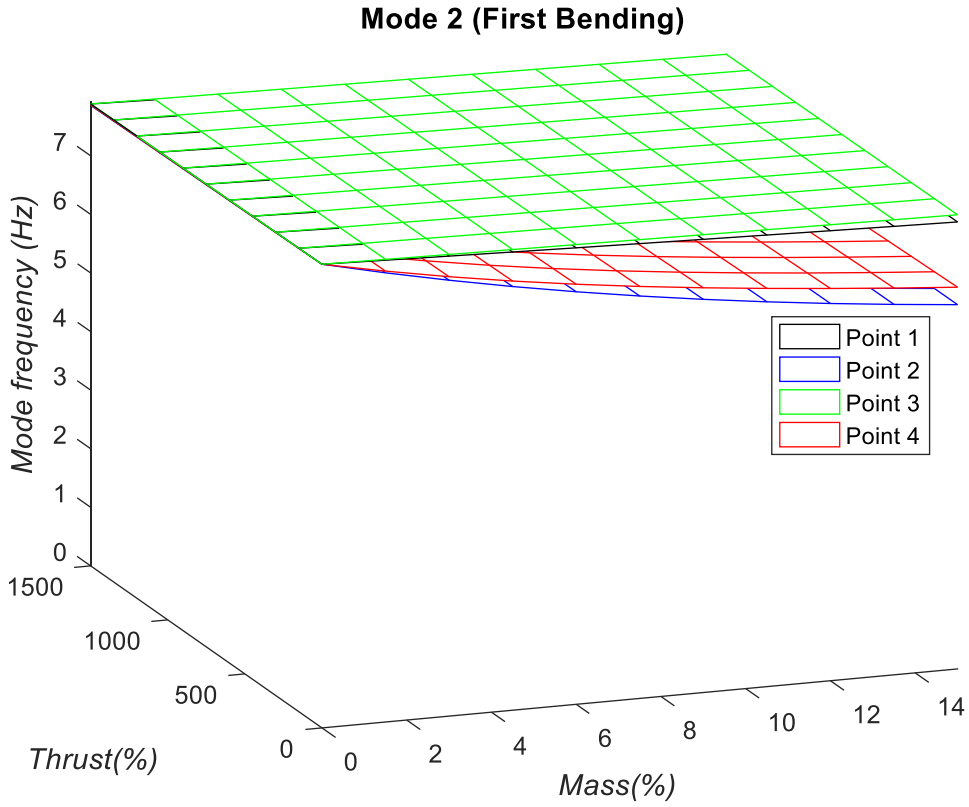

Figure 18-Mode 2 Frequency Variation with External Store Configuration and Position

Figure 18 shows how the first bending mode varies with external store mass, thrust, and position. The frequency of the mode for clean wing configuration is 7.915Hz. With the external store placed at point 1 or point 3 along the mid-span, the change in the mode frequency with external mass and thrust is negligible. The surfaces for points 2 and 4 also follow closely together and show negligible variation with external thrust. However, the mode frequency is seen to drop when the external mass is at these two wing-tip points.

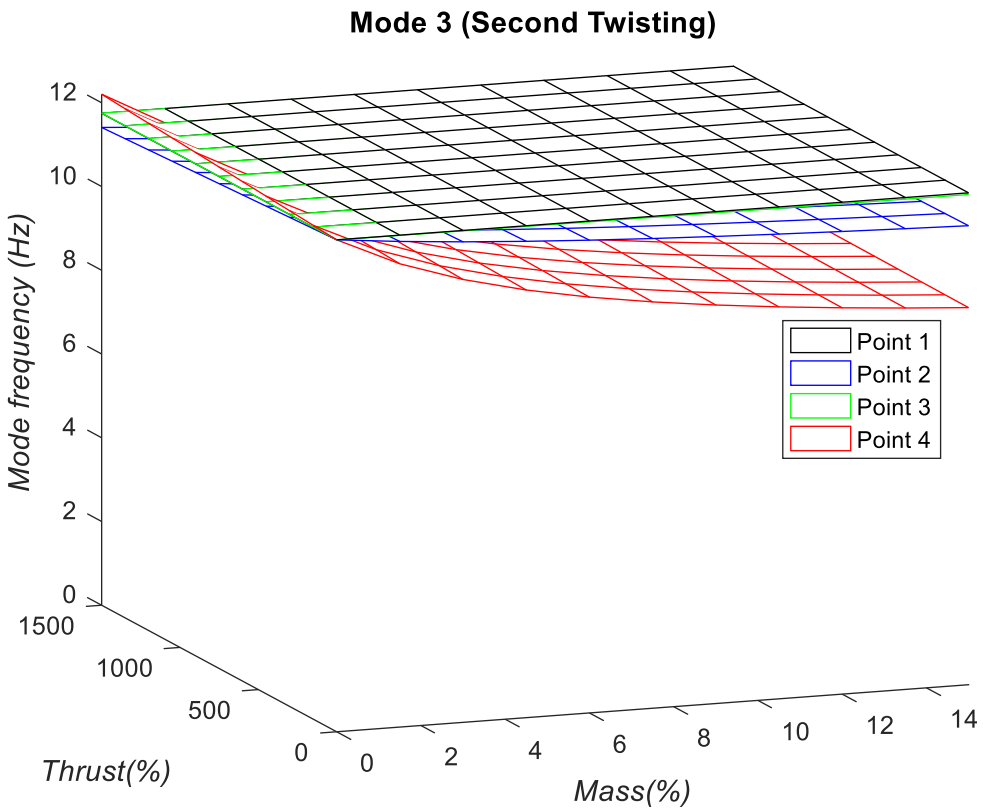

Figure 19-Mode 3 Frequency Variation with External Store Configuration and Position

Figure 19 shows how the second twisting mode varies at each of the four wing positions with external mass and thrust. The frequency of this mode for clean wing configuration is 11.75 Hz. With the external store placed at point 1 and 3, this mode does not vary at all with the mass or thrust of such a external store, maintaining the clean wing value. Along the leading and trailing edge of the wing-tip, point2 2 and 4, variation mainly occurs with external mass, particularly for point 4. For low values of external mass, some variation is seen at these two points with thrust.

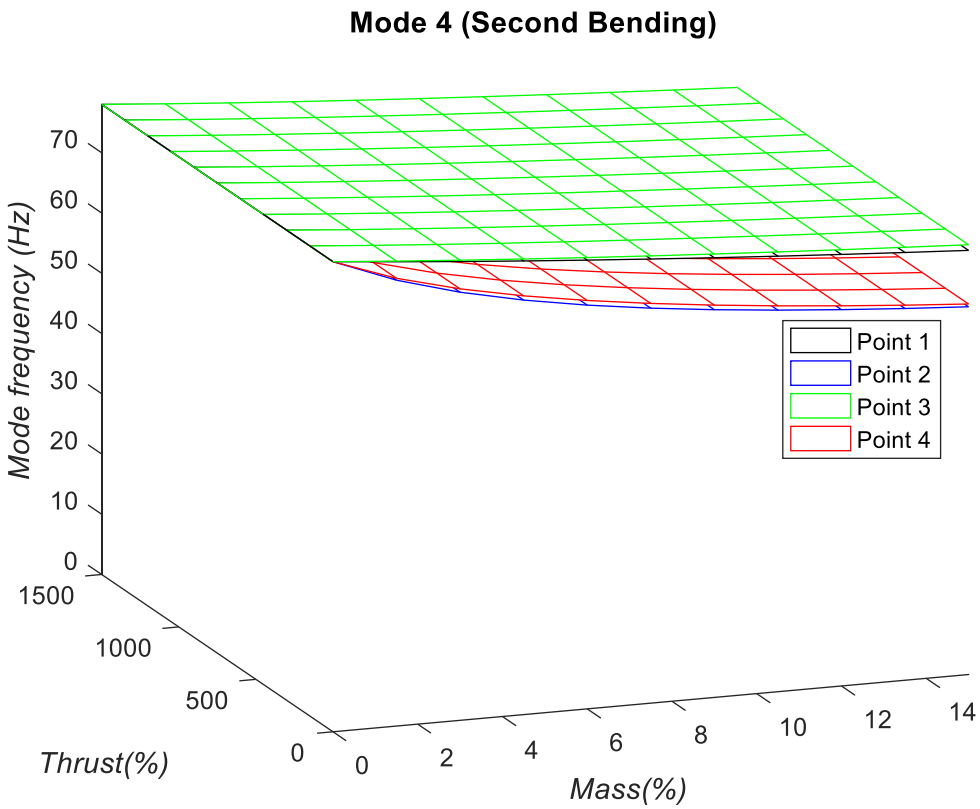

Figure 20-Mode 4 Frequency Variation with External Store Configuration and Position

Figure 20 shows how the frequency of the second bending mode varies with the external store mass and thrust and with the position of the external store. Once again, strong similarities can be drawn between points 1 & 3 and points 2 & 4. For all four store positions, no variation in the mode frequency is seen with increased external thrust. The mode frequency for clean wing configuration is 78.02 Hz. For positions 1 and 3 and the leading and trailing edges of the mid-span respectively, the mode frequency slightly reduces in a linear manner. At the wing-tip, stores placed along points 2 and 4 are seen to cause the frequency of this mode to fall sharper with the increased external mass.

5. Gust Response

The gust response calculations needed to be carried out at a given flight velocity which is below any instability speed. As seen in the previous section, this instability speed is dependent on the configuration of the wing system in relation to values of external mass and follower force present and the position of such external store, and so firstly the lowest possible instability speed is calculated for all possible external store locations at the set external mass and follower force values. Once this lowest instability speed is calculated for all possible external store locations, a flight velocity 20% below this value is used for the gust analysis. Thus, each of the plots was calculated at a different velocity. The five typical 1-cosine gusts used in this gust response analysis are represented in figure 21.

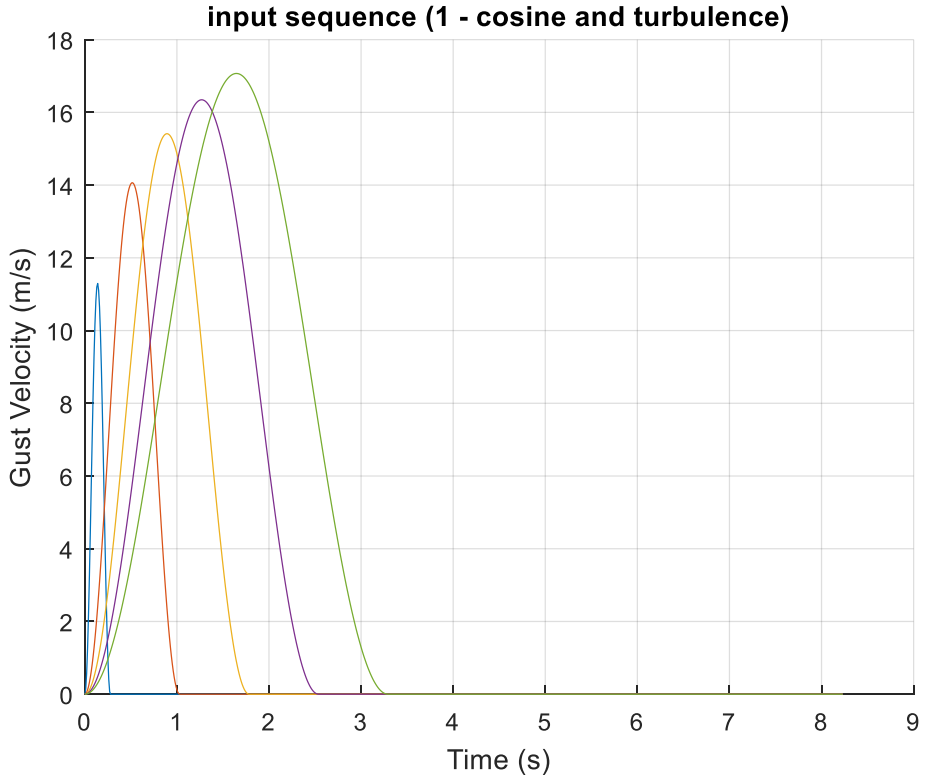

Figure 21-1-Cosine Gust Family

Using this velocity the gust analysis was then carried for each external store position in turn. For the first store location, the wing was subjected to the five 1-cosine gusts. The deflections of the wing-tip leading edge were computed and the maximum and minimum deflection values as shown in figure 22. The external store is then moved to the next station and maximum and minimum deflections again recorded. The following mesh plots show the maximum and minimum deflection for each of the external store locations.

As with the previous section, results are presented in three subsections in terms of external store configuration. In the first subsection, the external store takes the form of a point mass only. Secondly the effects of follower force or thrust position is presented. The final subsection presents the effects of the position of a point mass/follower force combination. Each subsection presents three plots with the magnitude of the mass and/or follower force increasing with each subsequent plot.

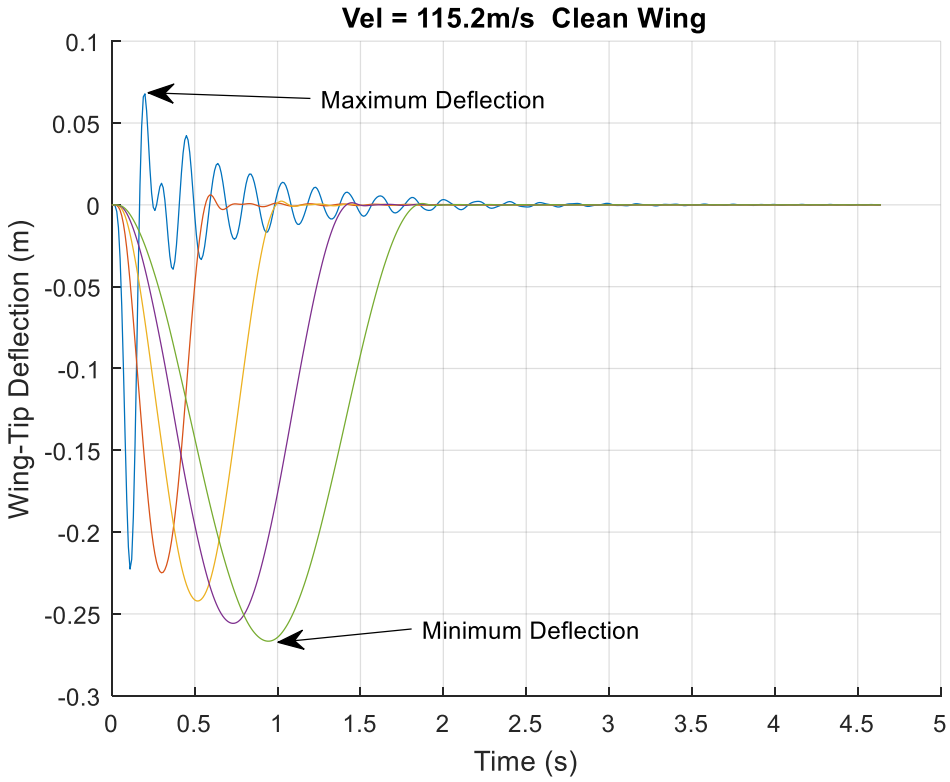

Figure 22-Wing Tip LE Deflection Gust Response

5.1. Wing with Point Mass

It is worth noting here that positive deflection represents downward displacement of the leading edge wing-tip relative the air flow, and vice versa for negative deflection. Figure 23 shows the effects of a point mass only of magnitude 5% the mass of the wing on the maximum and minimum deflection of the wing during the gust response. With the mass placed at the very root of the wing, the deflections is 0.06923 m which is equal to that of clean wing configuration at the given velocity of 108 m/s. The maximum deflection is seen to increase with span wise movement of the external mass. Maximum deflection with mass placed at the wing-tip varies significantly with chord wise placement. At the leading edge wing-tip, maximum displacement is around 0.0817 m and this increases as the mass is moved aft, reaching a maximum value of 0.1029 m at the 90% wing-tip chord. The smallest maximum

deflection occurs with the mass placed at the leading edge mid-span with a deflection of 0.06778 m, which is marginally less than the clean wing value. Minimum displacement in the negative direction in general is greater. Towards the very leading edge wing-tip minimum displacement dips to its lowest value of -0.2254 m. Negative deflection is reduced slightly when mass is placed at the 80% chord of the wing-tip where minimum deflection is -0.2251m.

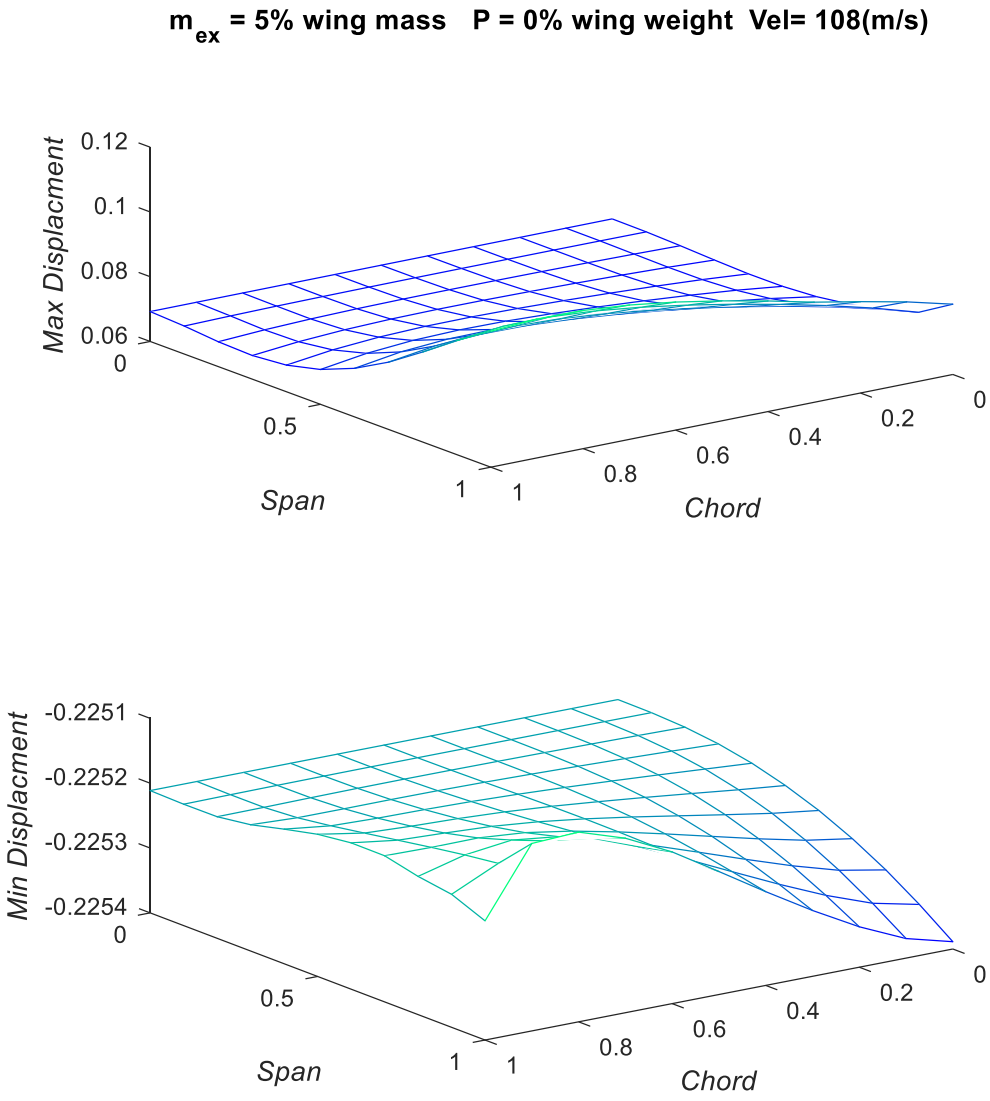

Figure 23-Wing-tip Deflection with Gust vs External Mass Location

Figure 24 shows the results of a gust response conducted at 74.4 m/s for a wing with a 10% wing mass and how the position of the mass changes the deflection of the wing during the gust. At the wing root maximum deflection is 0.0157m. The variation in maximum deflection is seen to remain constant with

span-wise movement of the mass up to the mid span. Beyond this mid-span station, the maximum deflation is seen to increase exponentially with span up to a maximum along wing-tip which also varies from a value of 0.03949m at the tip trailing edge to 0.04233m at the tip leading edge. Minimum deflections at the wing root starts at -0.1419m but from there follow a non-linear pattern but are most critical at the leading edge wing-tip where deflection is -0.142m.

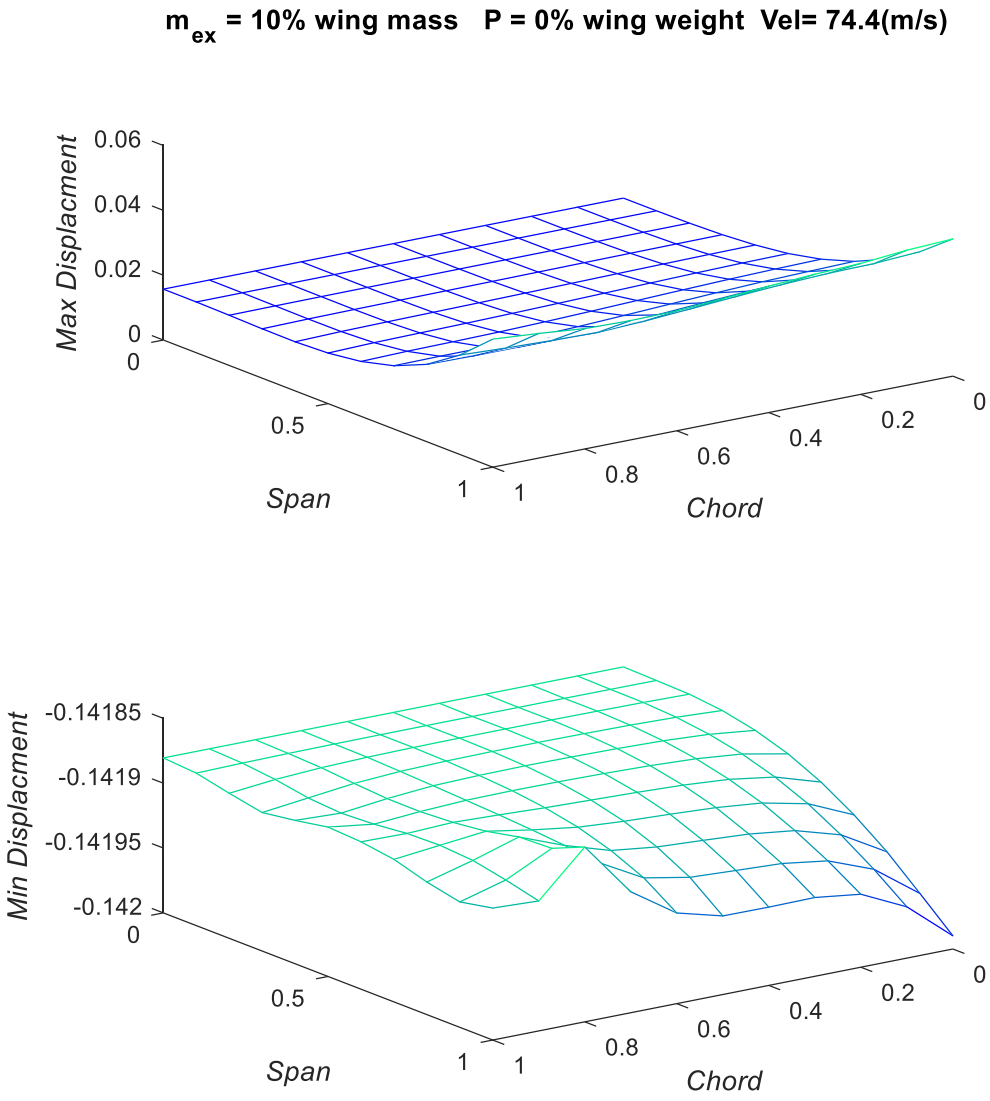

Figure 24-Wing-tip Deflection with Gust vs External Mass Location

Figure 25 plots the gust deflections of a wing with a 15% mass carried out at 61.6 m/s. At the wing root maximum deflection is 0.01023m. Only marginal change in maximum deflection is seen with span wise movement of the mass up to the mid span of the wing. Towards the front of the wing,

maximum deflection increases exponentially with span wise movement of the mass reaching its critical value of 0.0257m at the leading edge wing-tip. For the aft section, initially a drop in maximum deflection is seen. The smallest deflection value of 0.00551m occurs with the mass placed at the mid chord 80% span station. The minimum deflection changes very little with mass position but is slightly more pronounced when placed at the leading edge of the wing span which has a value around -0.1147m.

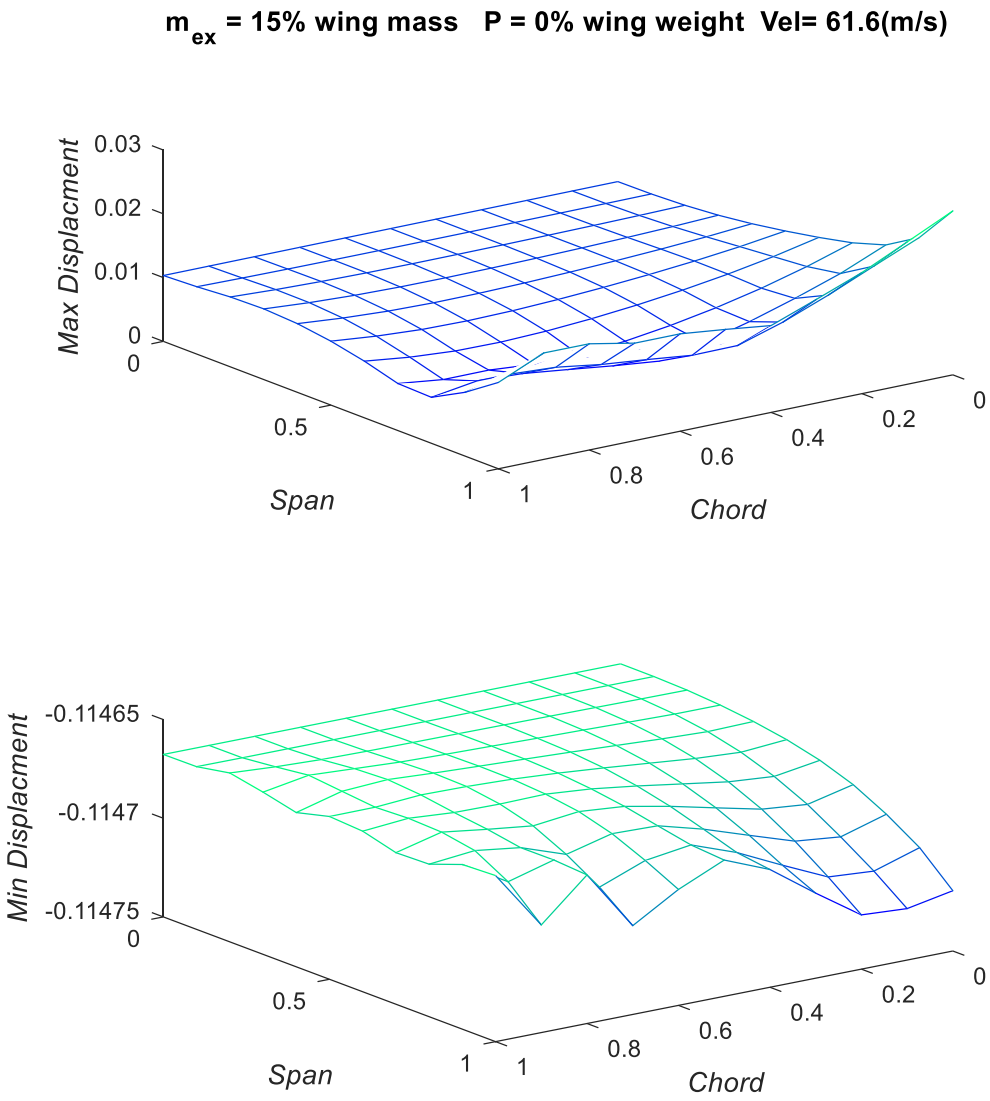

Figure 25-Wing-tip Deflection with Gust vs External Mass Location

5.2. Wing with Follower-Force

In this subsection results are shown for maximum and minimum deflection during a gust response at a velocity 80% below the minimum flutter speed for a wing with follower-force excluding external mass. Again, the magnitude of this follower-force increases incrementally. For a follower force or thrust with a magnitude equal to 500% the weight of the wing, the effect of thrust position on maximum and minimum wing-tip deflection for a gust response carried out at 105.6 m/s is shown in figure 26. Thrust placement at the wing root causes a maximum deflection of 0.06699m. Placement at the leading edge of the wing-tip reduces maximum deflection moderately to 0.06632m. Moving the thrust aft towards the trailing edge causes deflection to increase to 0.06989m.

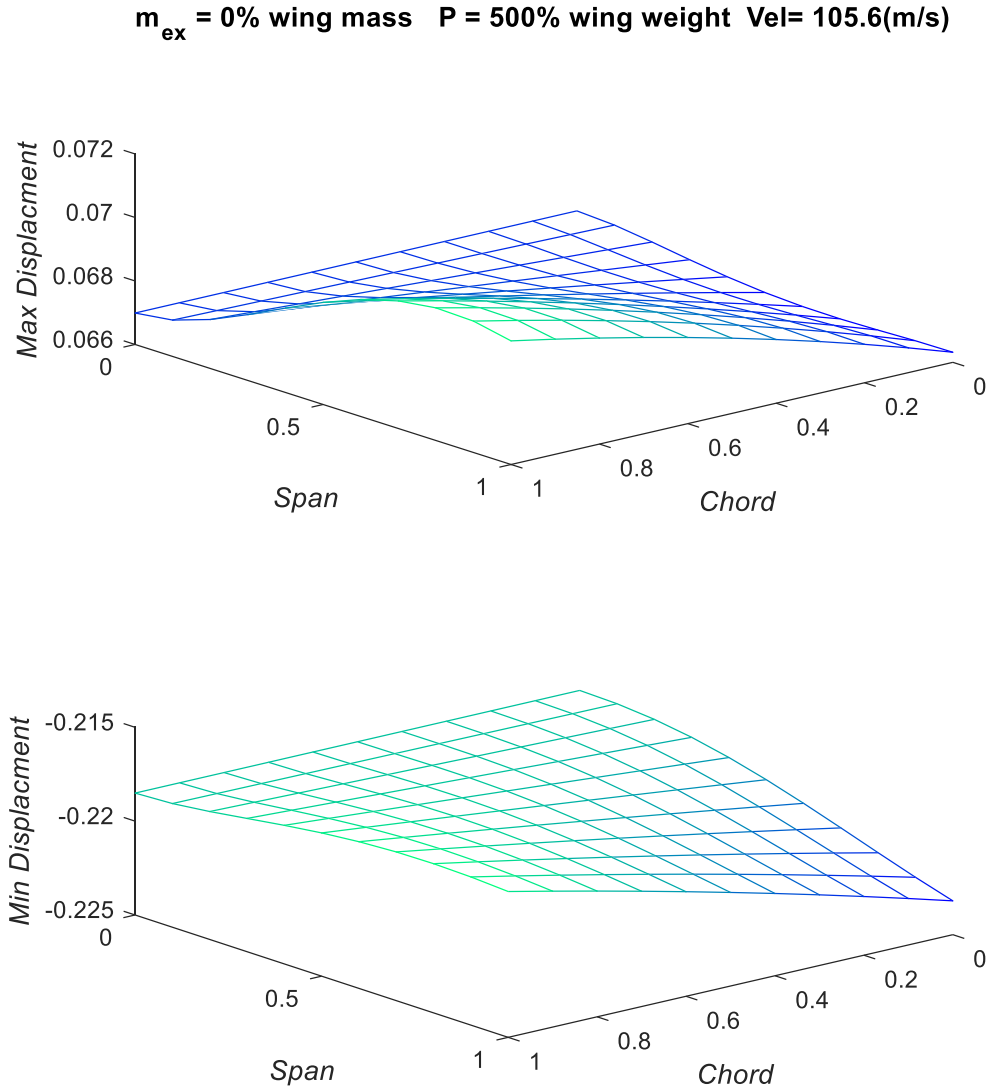

Figure 26-Wing-tip Deflection with Gust vs External Thrust Location

The critical position is slightly inbound from the wing-tip at the 80% span of the trailing edge where maximum deflection reaches 0.07018m. Negative deflection follows an inverse pattern to that seen with maximum deflection with the greatest amount of negative deflection occurring at the leading edge of the wing-tip, and the least amount of negative deflection occurring at the trailing edge 90% span with specific values been -0.2232m and -0.2172m respectively.

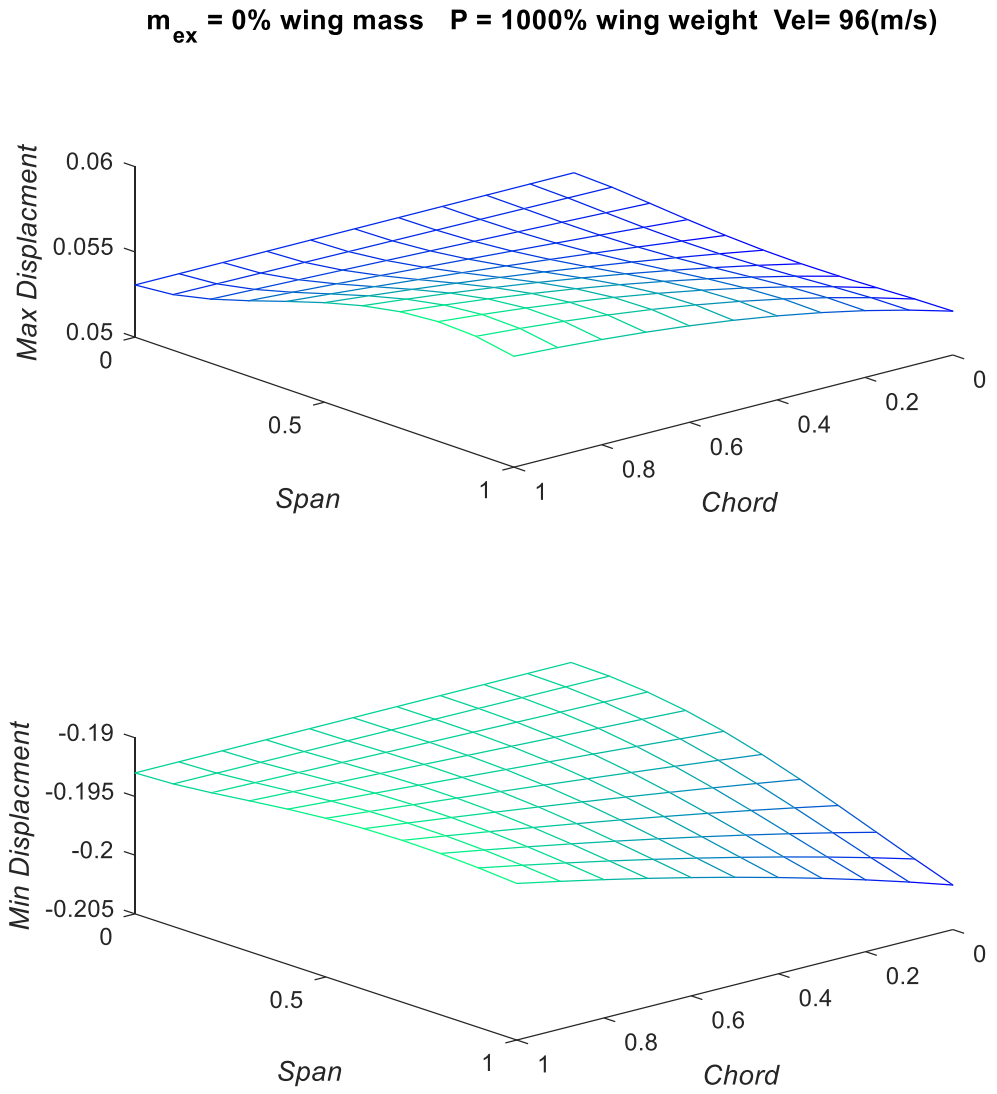

Figure 27-Wing-tip Deflection with Gust vs External Thrust Location

Figure 27 shows the wing deflections during a gust response at 96 m/s for a wing with point thrust of magnitude 1000% the wing weight. With the thrust placed at the wing root maximum and minimum deflections are 0.05306m and -0.193m respectively the maximum deflection is seen to increase to

0.05691m as thrust is positioned towards the trailing edge wing-tip area. However, this is the optimal thrust position in terms of minimum deflection. The minimum deflection reaches a minimum at the leading edge wig tip, reaching a value of -0.2012m at this position.

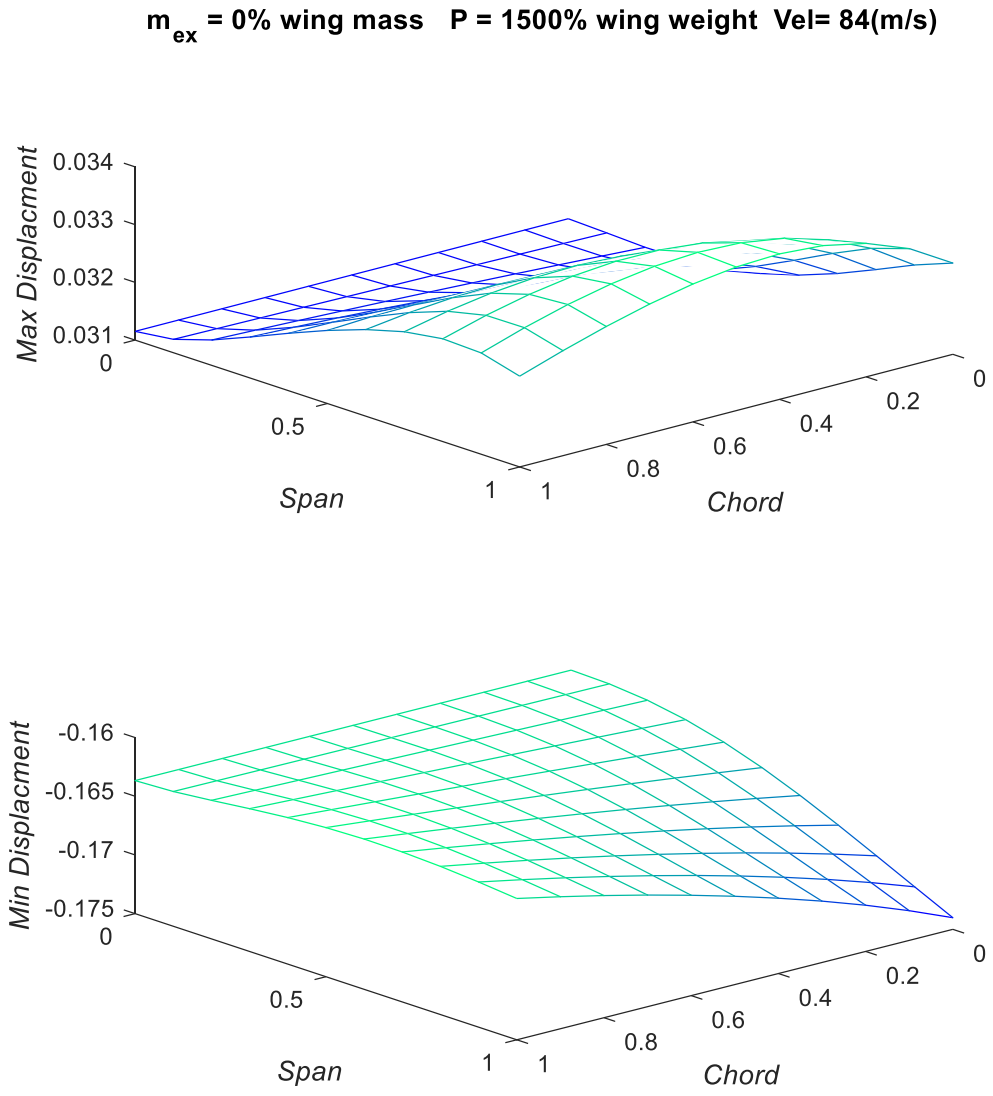

Figure 28-Wing-tip Deflection with Gust vs External Thrust Location

Figure 28 shows the effects the position a thrust 1500% the weight of the wing on the deflection of the wing during a gust response carried out at 84 m/s. The maximum deflection at the wing root is 0.03115m and minimum deflection is -0.1637m. Maximum deflection increases steadily with span wise movement of the thrust especially around the mid-chord of the wing. Deflection is most critical at the 40% chord of the wing-tip which has a deflection value of 0.03352m. Minimum deflection again

reaches its greatest negative value when the thrust is placed at the leading edge wing-tip. Here, minimum deflection reaches -0.174m. When the follower force is placed at the trailing edge, minimum deflection maintains a value very similar to when placed at the wing root.

5.3. Wing with Follower-Force and Mass

This subsection presents the results for the effects position of both external mass/thrust superimposed to a single store has on the wing-tip deflection during a gust response. The external mass and thrust is again increased incrementally for each subsequent plot.

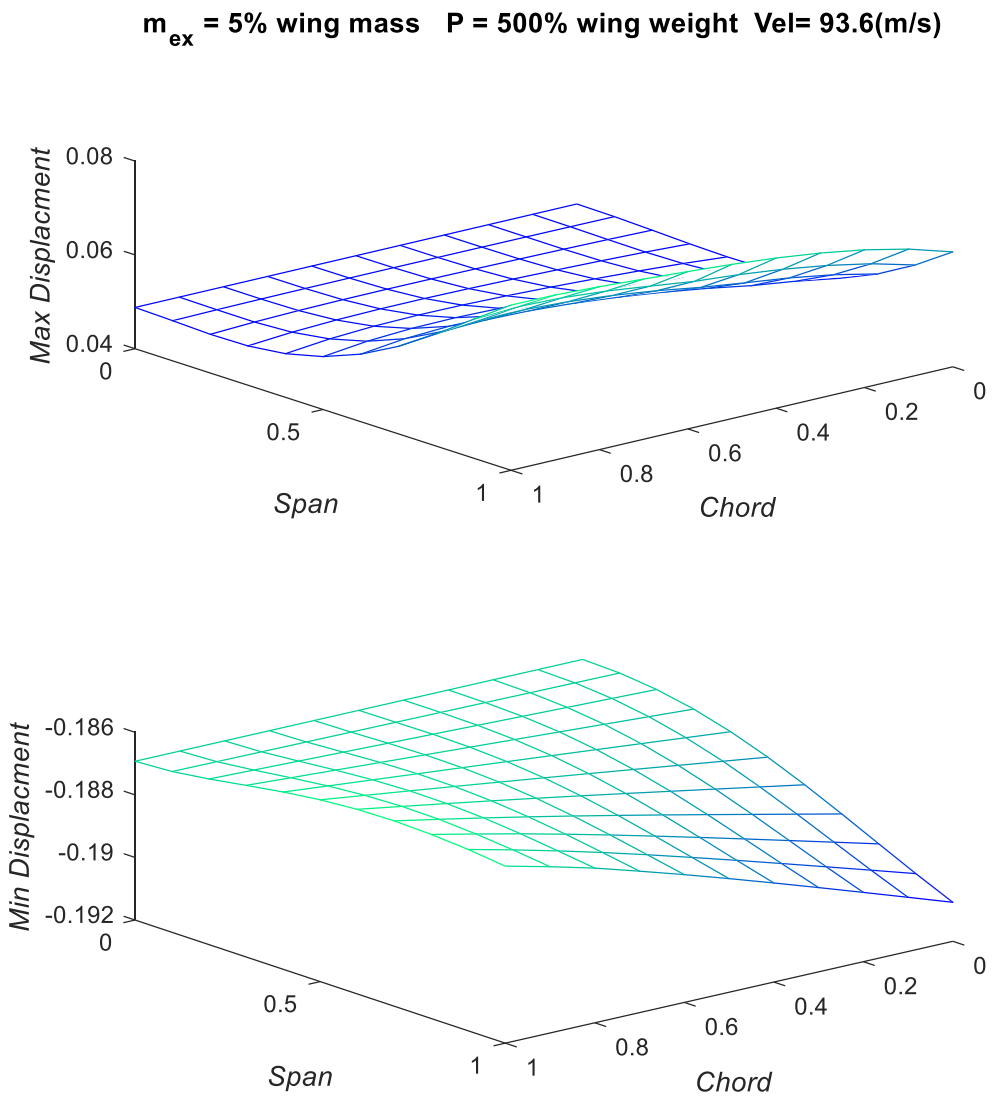

Figure 29-Wing-tip Deflection with Gust vs External Mass and Thrust Location

Figure 29 shows wing-tip deflections for a wing with external mass equal to 5% the mass of the wing and a lateral thrust equal to 500% the weight of the wing during a gust response at 93.6 m/s. At the root of the wing, maximum and minimum deflections caused by the external store is 0.04879m and -0.1869m respectively. From the root, moving the external store towards the wing-tip is seen to exponetially increases maximum deflection, particulalry along the trailing edge. The maximum deflection reaches its greatest value of 0.07523m at the trailing edge of the wing-tip. The minimum deflection is greatest at the leading edge wing-tip but improves slightly relative to wing root placement at the trailing edge. At the leading edge wing-tip negative deflection reaches -0.1908m and -0.1863m at the trailing edge wing-tip.

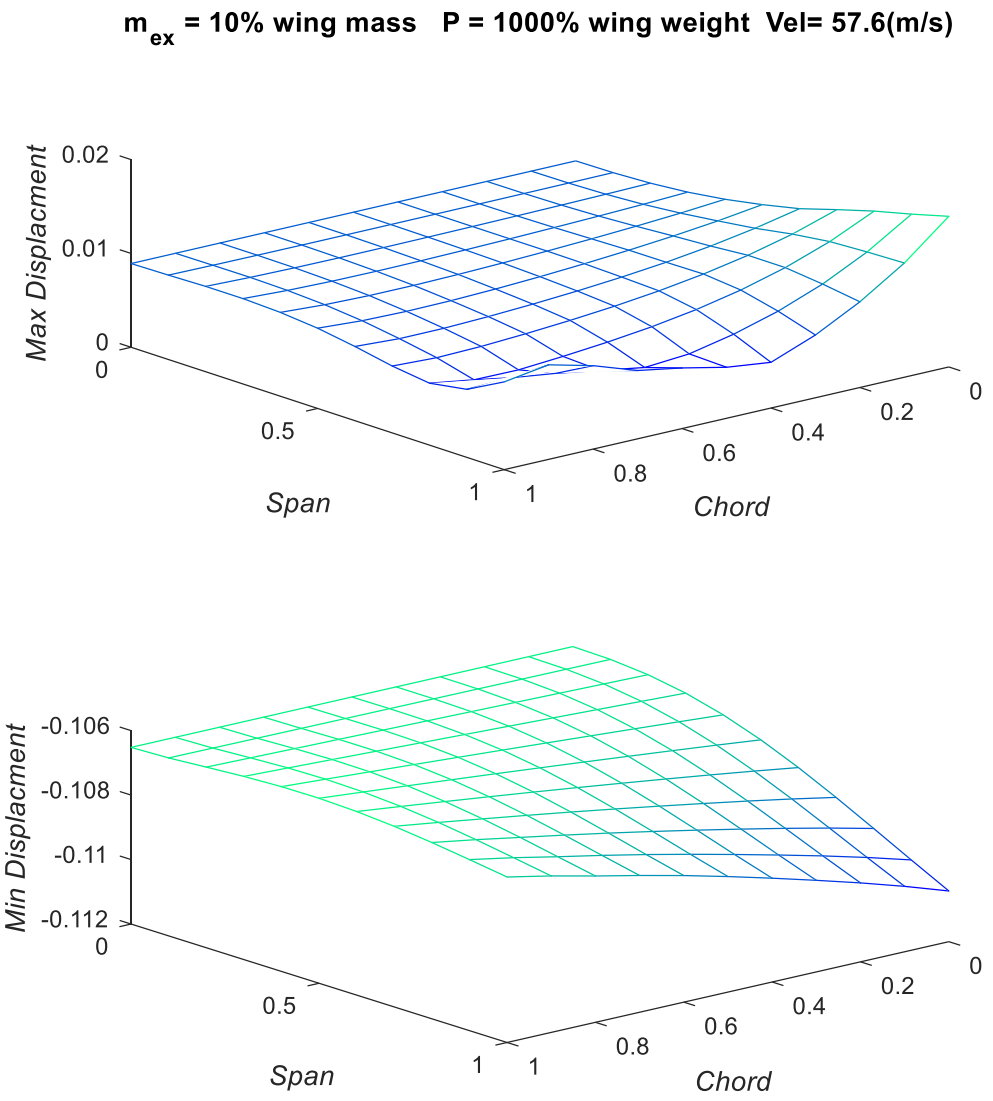

Figure 30-Wing-tip Deflection with Gust vs External Mass and Thrust Location

Figure 30 shows the wing deflections during a gust response carried out at 57.6 m/s. Maximum deflection with the external store placed at the wing root is 0.008924m and for the minimum deflection is -0.1065m. Very little change in maximum deflection is seen up to the 40% span. After this point, deflection is dependent on chord wise position. Towards the leading edge wing-tip, deflection increases to 0.01606m. Towards the trailing edge, deflection follows a distinctly non-linear pattern, initially dropping in value before increasing again. The lowest value of maximum deflection is 0.04871m at the 40% chord wing-tip station. The minimum deflection follows the usual pattern of increasing as the external store placed closer to the leading edge of the wing-tip. At this station the negative deflection reaches -0.1104m.

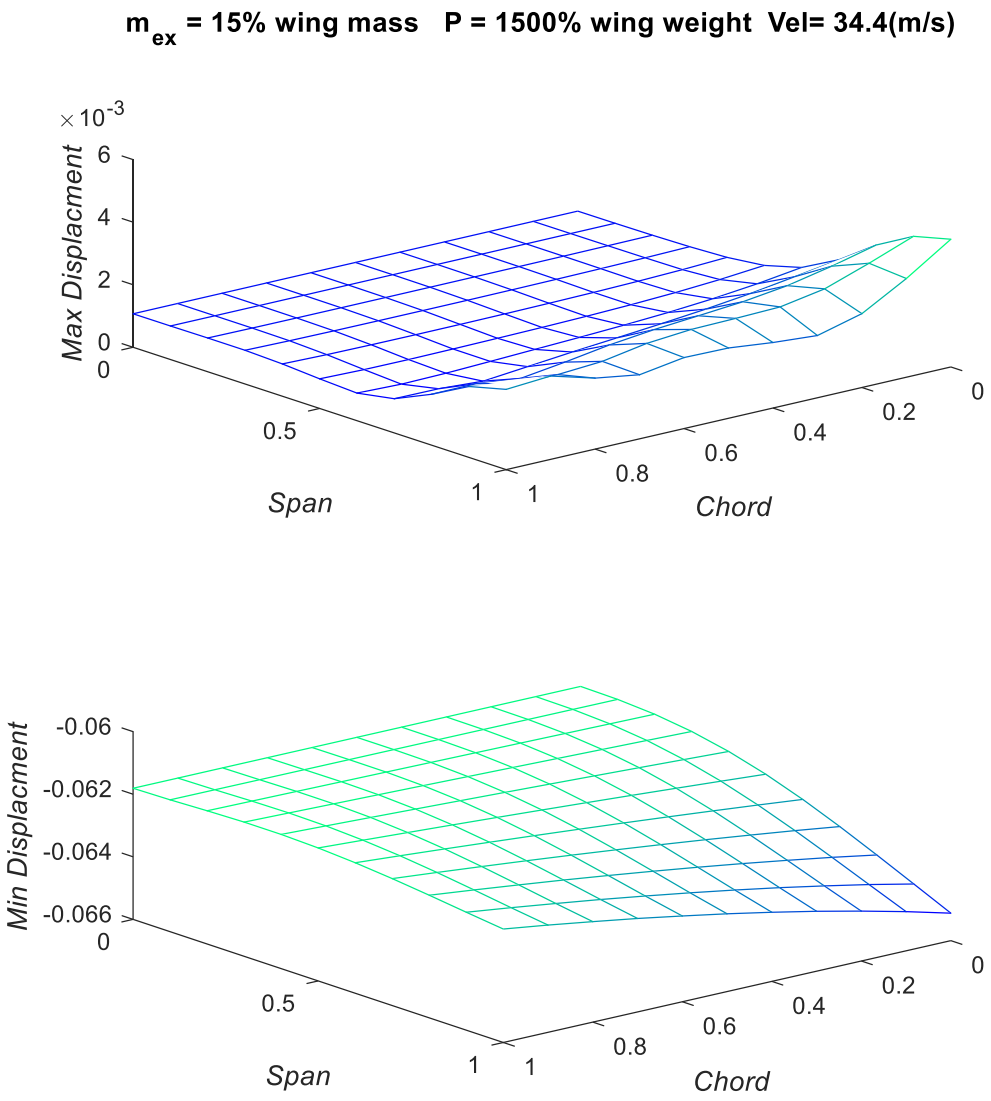

Figure 31-Wing-tip Deflection with Gust vs External Mass and Thrust Location

Figure 31 shows the effects the position an external store consisting of 15% wing mass and 1500% wing weight has on wing deflection during a gust response. The gust response is carried out at a velocity of 34.4 m/s. Along the wing root maximum and minimum deflections are 0.001071m and -0.06181m. Maximum deflection increases as the external store is moved towards the wing-tip particularly at the leading edge where the deflection is 0.004083m. The minimum deflection at the leading edge wing-tip is -0.06512m.

6. Discussion

Regarding the results for the effects of external mass on instability speed, it was seen that the position of such external mass plays a huge role on the wing's instability speed. Increasing the magnitude of the external mass serves to exaggerate effects, increasing or decreasing the instability speed further depending on the location of the mass. Moving the mass towards the wing root brings the instability speed closer to that of the clean wing. Mass placement toward the tip of the wing sees the most drastic changes in instability speed but is highly dependent on the chord wise position of the mass. Mass placement towards the leading edge of the wing-tip stabilised the wing significantly. The stability speed encountered with mass in this position would usually take the form of divergence speed. In contrast, external mass placement at the trailing edge and mid-section of the wing-tip brings flutter speed down to below that of clean wing values. Flutter frequency in general remains constant with change in mass position, apart from at the trailing edge of the wing-tip where flutter frequency is seen to drop in value.

Application of an external follower force also affects the instability speed; however, this effect is far smaller than that of external mass. In general this follower force plays a destabilising role. Moving follower force span wise in a direction of wing root to tip, initially has no effect up to around the 70% span. Beyond this towards the wing-tip, the flutter speed falls off moderately. Chord wise position of follower force also effects flutter speed along the wing-tip. Flutter speed is reduced most with follower force positioned at the leading edge of the wing-tip. The follower force position has very little effect of the flutter frequency, apart from at the trailing edge of the wing-tip which sees a slight increase in flutter frequency.

With external mass and thrust superimposed, the instability speed follows the same general pattern as for external mass only but with values across the wing reduced, particularly towards the wing-tip. As with external mass only, flutter frequency drops at the trailing edge wing-tip. At the leading edge of the wing-tip, mass has a great capacity to increase instability speed. However, at the trailing edge of the wing, external mass in limited in it stabilizing effect and can even reduce instability speed. Increasing the thrust moderately reduces instability speed at these areas.

The frequencies of the four normal modes were seen to vary with external store position and composition. Generally, the mode frequencies vary mostly with external mass which has the effect of reducing the frequencies in a roughly linear patter inversely proportional to the external mass. The first twisting mode is an exception to this which varies also with external thrust, particularly when placed along the trailing edge, and has the effect of increasing frequency. Span position of external stores plays a more important role on the mode frequencies compared to chord position.

The placement of external mass on the wing has a significant effect on the amount of deflection experienced during a gust response. In general, the greater the external mass, the less deflection occurs. Total deflection changes primarily with span location of the external mass, with greatest amount of deflection taking place towards the wing-tip. Smaller mass values result in more variation in gust deflections with mass position. In certain cases, a small external mass positioned at the wing-tip can cause gust deflection greater than that of the clean wing configuration. External thrust also serves to reduce deflection during gust response but is less sensitive to position. Very little variation in wing deflection is seen with change in thrust location. The reduction in deflection is also less than that for external mass. External stores consisting of mass and thrust reduce gust deflection most. Deflection values do however increase towards the wing-tip as was the case for external mass only.

The results uncovered in this thesis leaves room for further investigation. Particularly the first set of results which looked at the effects of an external stores position and magnitude on the instability speed of the wing. On these plots, it was seen that as the external mass was moved span wise from root to tip, a point was reached after which the shape of the plot became highly irregular. Referred to as the transition point, these nonlinearities occur sooner and more drastically for larger masses. Investigation into the physical/mechanical reasons behind these non-linear behaviours could prove useful.

Due to the superior reliability of electric motors compared with more conventional jet engines and so the likelihood of an engine out situation occurring, electric aircraft design configurations tend to have their main engines situated at the wing tips. Although these designs are still at risk of an engine out case, such as a bird strike, and often have a tail inadequate in size to deal with such a situation effectively, the results of this thesis are of particular relevance to these electric configurations.

7. Conclusions

The results of this thesis are highly relevant to the issues of improving aircraft efficiency and reducing gust loads. Firstly, it is mass placement which is the most important factor for wing flutter boundaries. External mass stores should be kept towards the leading edge of the wing-tip. In the design of wing structures, instability speed can be increased with a more effective mass distribution which concentrates mass at this leading edge wing-tip position. Engine thrust reduces instability speed, particularly at towards the wing-tip but this effect is usually negated by the effect of the mass of the engine.

In relation to gust response, external mass was seen to result in greater deflections of the wing. However, it was the smaller values of mass that resulted in the greatest wing deflection. The deflection was greater when the mass was placed towards the wing-tip. How the chord wise position of the mass affected the gust deflection also depended on the magnitude on the mass. For small values of mass, placement at trailing edge resulted in the greatest deflection. Conversely, for large values of mass the most deflection was seen when placed at the leading edge. The follower force resulted in only minor gust deflection but increased with larger forces and when placed towards the leading edge wing-tip.

In table 1, a divide in the various studies was found regarding how instability speed varies with span wise movement of external mass although good agreement was found regarding the effects of a wing mounted follower force. Regarding external mass, two general patterns emerged, the first being that flutter speed continuously increases as mass in moved span-wise from wing root towards wing-tip. This pattern most closely fits the results of this thesis. The second general pattern is for the flutter speed to drop as the external mass reaches mid-span, but increases to clean wing flutter speed as the wing-tip is approached. A possible explanation for this can be found in the report by Runyan (1980). In this report, results were presented for variation in flutter speed with span wise position of external mass for two cases. The first case uses the assumption of a flexible mass pylon, and the second case assuming a rigid pylon. The flexible pylon results fit that of the first pattern, and the rigid pylon results fit the second. This indicates that the discrepancies in the results of past work could be caused, even if partly, by whether pylon is assumed to be rigid or flexible or how this pylon is incorporated into the model.

8. Future Work

The results obtained in this thesis were obtained under the assumption that the bending and torsional stiffness of the system are held constant. Future work could focus on exploring the effects of bending and torsional stiffness in relation to external store position. The divide in the results of previous work regarding the effects of flutter speed and external mass, outlined in table 1, could potentially be explained by whether the model used a rigid or flexible pylon, but further work is needed to explore this area further so as to determine if this is the cause of the discrepancy seen in the results.

9. References

1 Wright, J. R. & Cooper, J. E. (2007), Introduction to Aircraft Aeroelasticity and Loads, John Wiley and Sons.

2 Fuller, F.B (1995), Evolution of Aeroplane Gust Loads Design Requirements, *Journal of Aircraft, vol32 n2 pp235 – 246.*

3 Flomenhoft, H.I. (1994), Brief History of gust models for aircraft design, *Journal of Aircraft, vol31 n5 pp1225 – 1227.*

4 High Level Group on Aviation Research (2011) *Flighpath2050 Europe's Vison for Aviation*, [Online] Report Number: EUR 098 EN. Luxembourg, European Union. Available from: https://ec.europa.eu/transport/sites/transport/files/modes/air/doc/flightpath2050.pdf [Accessed 14 September 2018].

5 Aerospace Technology Institute (2016), *Rising Ambition- Technology Strategy and Portfolio update 2016*, [Online] Available from: https://www.ati.org.uk/wp-content/uploads/2017/10/Raising-Ambition-ATI-Technology-Strategy-Portfolio-Update-2016.pdf [Accessed 16 September 2018].

6 Greitzer, E.M. et al. (2010), *N+3 Aircraft Concept Designs and Trade Studies Final Report, NASA, Volume 1*.

7 Bradley, M.K. & Droney, C.K. (2012), *Subsonic Ultra Green Aircraft Research Phase II: N+4 Advanced Concept Development, NASA.*

8 Kuzmina, S. et al., (2002), Review and outlook on active and passive aeroelastic design concept for future aircraft, *ICAS 2002 Congress8-13 September 2002, Toronto, 432, pp 1–10.*

9 Miller, S. Vio, G.A. Cooper, J.E. Vale, J. Luz da, L. Gomes, A. Lau, F. Suleman, A. Cavagna, L. De Gaspari A. Ricci, S. Riccobene, L. Scotti, A. Terraneo, M. (2010), *SMorph – Smart Aircraft Morphing Technologies Project*, AIAA, 2010-2742.

10 Barbarino, S. Bilgen, O. Ajaj, R.M. Friswell, M.I. Inman, J.D. (2011), A Review of Morphing Aircraft, *Journal of Intelligent Material Systems and Structures*, Vol. 22, Issue 9.

11 Reich, G. & Sanders, B. (2007), Introduction to Morphing Aircraft Research, *Journal of Aircraft*, Vol. 44, No. 4, 1059-1059.

12 NASA Graphic / NASA Langley/Advanced Concepts Lab (2018) A*rtist's concept of NASA's X-57 Maxwell aircraft* [Online] Available from: https://www.nasa.gov/centers/armstrong/news/FactSheets/FS-109.html [Accessed 21 February 2019].

13 Goland, M. & Luke, Y.L. (1948), The flutter of a uniform wing with tip weights, *Journal of Applied Mechanics 15.*

14 Runyan, H.L. & Sewall, J. (1948), Experimental Investigation Of The Effects Of Concentrated Weights On Flutter Characteristics Of A Straight, *NACA Technical Note No.1594.*

15 Runyan H.L. & Watkins C.E. (1949), *Flutter of a Uniform Wing with an Arbitrarily Placed Mass According to a Differential-Equation Analysis and a Comparison with Experiment*.

16 Runyan H.L. (1950) *Experimental Investigation of the Effects of Concentrated Weights on Flutter Characteristics*

17 Feldt, W.T. & Herrmann, G. (1974), Bending- Torsional Flutter of a Cantilevered Wing Containing a Tip Mass and Subjected to a Transverse Follower Force, Journal Vol. 297, No. 6.

18 Hodges, D.H., Patil, M.J., Chae, S. (2001), Effect Of Thrust On Bending-Torsion Flutter Of Wing, *AIAA 2001-1656.*

19 Runyan, H.L, (1980), *Effect of a Flexibly Mounted Store on the Flutter Speed of a Wing, NASA Contractor Report.*

20 Fazelzadeh, S.A, et al, (2009), Bending-torsional flutter of wings with an attached mass subjected to a follower force, *Journal of sound and vibration.*

21 Wang, L., Wan, Z., Wu, Q., Yang, C., (2011), Aeroelastic modeling and analysis of the wing/engine system of a large aircraft, *Procedia Engineering 31,* 879-885.

22 Mazidia A., H. Kalantarib H., Fazelzadeh S.A., (2013), Aeroelastic response of an aircraft wing with mounted engine subjected to time-dependent thrust, *Journal of Fluids and Structures 39*, 292-305.

23 Mazidi, A. & Fazelzadeh, S.A. (2013), Aeroelastic Modeling and Flutter Prediction of Swept Wings Carrying Twin Powered Engines, *Journal Of Aerospace Engineering, Vol. 26, No. 3,1st July,* pp 586-593.

24 Fazelzadeh S.A., Marzocca P., Mazidi, A., Rashidi, E. (2009), Divergence and flutter of shear deformable aircraft swept wings subjected to roll angular velocity, *Acta Mech 212 (2010), 151–165,* PP 151–165.

25 Mazidi, A. & Fazelzadeh, S.A. (2011), Flutter of Aircraft Wings Carrying a Powered Engine Under Roll Maneuver, *Journal Of Aircraft, Vol. 48, No. 3, May–June 2011,*pp

26 Fazelzadeh S.A., Ghasemi A., Mazidi A. (2015), *Aeroelastic Analysis of Unrestrained Aircraft Wing with External Stores Under Roll Maneuver, International Journal of Acoustics and Vibration, Vol. 21, No. 3, 2016,* pp. 327-333.

27 Gern, H.F. & Librescu, L. (1998), Effects of externally mounted stores on aeroelasticity of advanced swept cantilevered aircraft wings, *Aerospace Science and Technology No.5,* pp 321-333.

28 Librescu, L. & Song, O. (2008), Dynamics of Composite Aircraft Wings Carrying External Stores, *AIAA Journal Vol. 46, No. 3, March 2008,* PP 568-577.

29 Mazidi, A. & Fazelzadeh, S.A. (2010), Flutter of a Swept Aircraft Wing with a Powered Engine, *Journal of Aerospace Engineering, October 2010,* pp. 243-250.

30 Amoozgar, M.R., Irani, S., Vaziry, M.A., Fate, A.R. (2011), *Flutter Characteristics Of A Composite Wing Containing An Arbitrary Concentrated Mass, Iranian Aerospace Society Conference March 1-3/2011.*

31 Tang, D. & Dowell, E.H. (2002), *Limit-cycle hysteresis response for a high-aspect-ratio wing model. J Aircraft 39,* pp 885–888.

32 Dowell, E., Edwards, J. & Strganac, T. (2003), *Nonlinear aeroelasticity. J Aircraft 2003; 40: 857–874.*

33 Kim, K. & Strganac, T. (2003), *Nonlinear responses of a cantilever wing with an external store, paper no. AIAA-2003-1708, pp.1–15. Norfolk, VA: AIAA/ ASME/ASCE/AHS/ASC.*

34 E. Zafari et al, (2017), Analytical nonlinear flutter and sensitivity analysis of aircraft wings subjected to a transverse follower force, *Proc IMechE Part G: J Aerospace Engineering 0(0) 1–13 IMechE 2018.*

35 Becker, J. (1986), Prediction and Alleviation on a Fighter Aircraft, *Advisory Group for Aerospace Research and Development, AGARD-R-728.*

36 Fazelzadeh, S.A, Azadi, M., Azadi, E. (2017), Suppression of nonlinear aeroelastic vibration of a wing/store under gust effects using an adaptive-robust controller, *Journal of Vibration and Control, Vol.23,* pp 1206-1217.

37 EASA (2007), *Certification Specifications for Large Aeroplanes CS-25,* [Online] Available from: https://www.easa.europa.eu/sites/default/files/dfu/CS-25_Amdt%203_19.09.07_Consolidated%20version.pdf

38 Housner, J. M. and Stein, M. (1974), Flutter analysis of swept-wing subsonic aircraft with parameter studies of composite wings, *NASA TN. D-7539, National Aeronautics and Space Administration, Washington, DC.*

39 Patil, M. J., and Hodges, D. H. (2000), Nonlinear aeroelastic analysis of composite aircraft in subsonic flow, *J. Aircr., 37(5),* pp 753–760.

40 Qin, Z., and Librescu, L. (2003), Aeroelastic instability of aircraft wings modeled as anisotropic composite thin-walled beams in incompressible flow, *J. Fluids Structures, 18(1),* pp 43–61.

41 Fazelzadeh, S.A., Marzocca, P., Rashidi,E., and Mazidi,A.(2010), Effects of rolling maneuver on divergence and flutter of aircraft wings carrying an external store, *J. Aircr., 47(1),* pp 64–70.